Electronic Supplementary Material (ESI) for ChemComm.

Electronic Supplementary Information for:

Consequences of conformational flexibility in hydrogen-bond driven self-assembly processes

José Augusto Berrocal,‡[a] Florent Di Meo,‡[b,c] Miguel García-Iglesias,‡[a] Ronald P. J. Gosens,[a] E. W. Meijer,[a] Mathieu Linares*[b,d] and Anja R. A. Palmans*[a]

[a] Institute for Complex Molecular Systems, Eindhoven University of Technology, P. O. Box 513, 5600 MB Eindhoven, The Netherlands. E-mail: a.palmans@tue.nl.

[b] Department of Physics, Chemistry and Biology (IFM), Linköping University, SE-581 83 Linköping, Sweden. E-mail: mathieu@ifm.liu.se

[c] INSERM UMR 850, Univ. Limoges, School of Pharmacy, 2 rue Dr. Marcland, F-87025 Limoges, France

[d] Swedish e-Science Research Centre (SeRC), Linköping University, SE-581 83 Linköping, Sweden

‡ These authors have contributed equally

Table of contents

Experimental details ESI3

^{1}H NMR, ^{13}C NMR, IR, MALDI-TOF-MS spectra and DSC characterization of **1** and **2** ESI8

Polarized Optical Microscopy characterization ESI16

Temperature dependent IR ESI17

Concentration dependent gelation studies ESI18

Solution-phase IR ESI19

Study of the self-assembly of **2** in MCH with ^{1}H NMR spectroscopy ESI20

Transmission Electron Microscopy characterization ESI21

UV-Vis and CD spectra ESI23

Tempeature Dependent UV-Vis and CD spectra in Heptane ESI24

Dynamic Light Scattering characterization ESI25

Computational section ESI26

References ESI36

Experimental details

Materials

Unless stated otherwise, all reagents and chemicals were obtained from commercial sources at the highest purity available and used without further purification. All solvents were of AR quality and purchased from Biosolve. Flash chromatography was performed on a Biotage flash chromatography system using 200–425 mesh silica gel (Type 60A Grade 633). Reactions were followed by thin-layer chromatography (precoated 0.25 mm, 60-F254 silica gel plates from Merck).

Instrumentation

^{1}H NMR and ^{13}C NMR spectra were recorded either on a Varian Mercury Vx 400 MHz (100 MHz for ^{13}C) or Varian Oxford AS 500 MHz (125 MHz for ^{13}C) NMR spectrometers. Chemical shifts are given in ppm (δ) values relative to residual solvent or tetramethylsilane (TMS). Splitting patterns are labelled as s, singlet; d, doublet; t, triplet; q, quartet; m, multiplet.

Matrix assisted laser desorption/ionisation mass spectra were obtained on a PerSeptive Biosystems Voyager DE-PRO spectrometer or a Bruker autoflex speed spectrometer using α-cyano-4-hydroxycinnamic acid (CHCA) and 2-[(2E)-3-(4-tert-butylphenyl)-2-methylprop-2-enylidene]malononitrile (DCTB) as matrices.

Infrared spectra were recorded on a Perkin Elmer Spectrum One 1600 FT-IR spectrometer or a Perkin Elmer Spectrum Two FT-IR spectrometer, equipped with a Perkin Elmer Universal ATR Sampler Accessory. Variable temperature IR was recorded on a Bruker Tensor 27 equipped with a PIKE GladiATR. Solution FT-IR measurements were performed using a CaF2 Liquid Cell with 0.05 mm pathlength purchased from New Era Enterprises.

Ultraviolet-visible (UV-vis) absorbance spectra were recorded on and a Jasco V-650 UV-vis spectrometer with a Jasco ETCT-762 temperature controller.

CD measurements were performed on a Jasco J-815 spectropolarimeter and the sensitivity, time constant and scan rate were chosen appropriately. Corresponding temperature dependent measurements were performed with a Jasco PTC-348WI Peltier-type temperature controller, with a temperature range of 273–353 K and adjustable temperature slope.

Polarization optical microscopy measurements were done using a Jenaval polarization microscope equipped with a Linkam THMS 600 heating device, with crossed polarizers.

DSC measurements were carried out with a PerkinElmer Pyris 1 DSC under a nitrogen atmosphere with heating and cooling rates of 10 K/min.

Dynamic light scattering measurements were performed on a Malvern mV Zetasizer equipped with an 830 nm laser.

Transmission Electron Microscopy was performed on a FEI company Tecnai G2 Sphera, operating at a voltage of 200 kV. For the analysis of the mBTA transfer to EM grids, micrographs were recorded on a CCD chip with 1024×1024 pixels, with pixel size corresponding to 22 nm.

Methods

UV-Vis and CD experiments were performed using quartz cuvettes with different optical paths (1 cm, 0.1 cm and 0.01 cm). Samples were prepared as follows: a stock solution of the desired mBTA derivative was prepared in the appropriate solvent and a calculated volume of such solution was diluted in cuvette to obtain the desired final concentration.

TD-IR was performed by drop casting a concentrated solution of mBTAs **1** and **2**, followed by solvent evaporation and a quick heating and cooling cycle (30 ºC/min). Once the sample had reached room temperature, IR was measured upon slow heating and cooling (10 °C/min).

Samples for solution FT-IR were prepared by dissolving the desired mBTA derivative in the desired solvent (sometimes heating or sonication was required). The solution was injected into the FT-IR Cell (pathlength 0.05 mm) with a syringe.

Samples for Polarized Optical Microscopy imaging were deposited on glass cover slips, heated up above the isotropic melt and slowly cooled down (10 °C/min).

Samples for Transmission Electron Microscopy imaging were prepared as follows: 7.5 mM solutions of **2** in heptane and MCH were drop cast on 400 mesh carbon film Cu TEM grids (Agar scientific) and air dried. Then, a 5 μL droplet containing a 2 wt% uranyl acetate water solution was applied for 15 seconds. The excess water solution was removed with a tissue.

Samples were left to dry overnight in a grid holder at room temperature and measured the day after.

Gelation experiments were performed as follows: compound **1** or **2** were weighed in a screw-cap 2 mL GC vial and the required amount of solvent (to obtain the desired wt % composition) was injected. Vials were sealed and heated up with a heat gun until a clear, transparent solution was obtained. The solutions were slowly cooled to room temperature and the gelation was qualitatively assed by inversed vial test.

Samples for Dynamic Light Scatttering were prepared by filtering solutions through a 0.2 mm PVDF-filter (Whatman) in a fluorescence cell with a path length of 1 cm. Solvents used in the experiments were previously filtered with 0.2 mm PVDF-filters (Whatman). Blanks were always measured before the actual measurements to confirm the absence of dust.

Synthesis of mBTAs 1 and 2

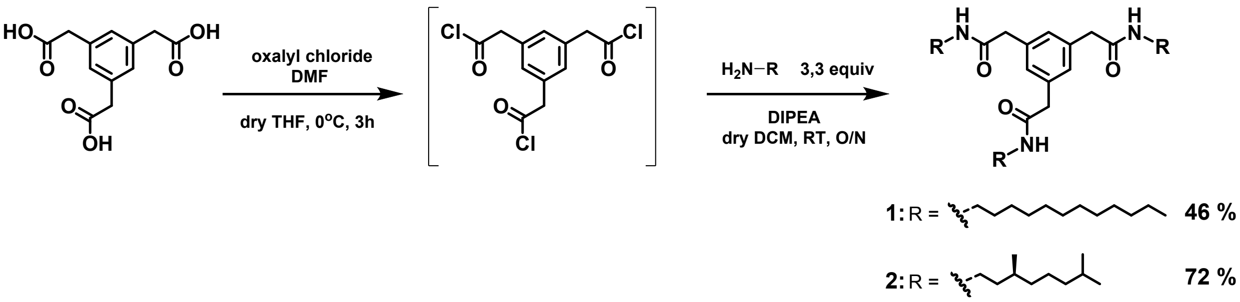

Scheme S1. Synthetic approach to mBTAs **1** and **2**.

Benzene-1,3,5-triacetic acid (788 mg, 3.12 mmol) was dissolved in dry THF (40 mL) and cooled to 0 ºC with an ice bath. After addition of one drop of DMF, oxalyl chloride (1.428 g, 11.25 mmol), previously dissolved in dry THF (10 mL), was added drop-wise in 10 minutes. After stirring for 3 hours, the volatiles were removed in vacuo. The crude material was redisolved in dry DCM (40 mL) and cooled to 0ºC with an ice bath. 3.3 mol equivalents of amine and DIPEA (2.019 g, 15,62 mmol) were dissolved in dry DCM (10 mL) and were added dropwise in 10 minutes. The mixture was stirred at room temperature under an argon atmosphere for 18 hours, after which the solvent was removed. The remaining residue was dissolved in chloroform (100 mL) and subsequently washed with 1M HCl (2 x100 mL) and 1M NaOH (1 x 100 mL). The organic phase was dried over Na_2SO_4, fitered and evaporated. The product was obtained after recrystallization in ethyl acetate (50 mL), followed by column chromatography performed with the Biotage Flash Chromatography purification system (SiO_2, eluent $CHCl_3$:MeOH from 97:3 to 95:5 in 6 Column Volumes). Yields: 46% for **1**, 72% for **2**.

2,2',2''-(benzene-1,3,5-triyl)tris(N-dodecylacetamide) (**1**)

^{1}H NMR (400 MHz, $CDCl_3$) δ: 7.08 (s, 3H), 5.51 (t, J = 8 Hz, 3H), 3.51 (s, 6H), 3.20 (q, J = 8 Hz, 6H), 1.47-1.24 (m, 60 H), 0.88 (t, J = 8 Hz, 9H).

^{13}C NMR (100 MHz, $CDCl_3$) δ: 170.52, 136.39, 129.43, 43.60, 40.02, 32.07, 29.81, 29.80, 29.76, 29.71, 29.69, 29.51, 29.43, 27.05, 22.84, 14.28.

FT-IR (ATR) ν: 3281, 3083, 2956, 2917, 2850, 1636, 1549, 1467, 1435, 1377, 1334, 1312, 1260, 1247, 1161, 721, 581.

UV-Vis [CH_3CN, λ (nm), ε ($L\times mol^{-1}\times cm^{-1}$)]: 200 (max, 43550), 224 (shoulder, 10802)

MALDI-TOF-MS calculated for $[C_{48}H_{87}N_3O_3]+Na^+$ 776,66 Da, found 776,65 *m/z*.

2,2',2''-(benzene-1,3,5-triyl)tris(N-((S)-3,7-dimethyloctyl)acetamide) (**2**)

^{1}H NMR (400 MHz, $CDCl_3$) δ: 7.06 (s, 3H), 5.57 (t, J = 8 Hz, 3H), 3.48 (s, 6H), 3.27-3.17 (m, 6H), 1.55-1.04 (m, 42H), 0.86 (d, J = 8 Hz, 9H), 0.85 (d, J = 8 Hz, 18H).

^{13}C NMR (100 MHz, $CDCl_3$) δ: 170.54, 136.33, 129.39, 43.54, 39.34, 38.19, 37.22, 36.75, 30.93, 28.07, 24.79, 22.84, 22.74, 19.60.

FT-IR (ATR) ν: 3288, 3083, 2954, 2925, 2869, 1643, 1543, 1460, 1417, 1378, 1365, 1351, 1247, 1169, 731, 578.

UV-Vis [CH_3CN, λ (nm), ε (L×mol^{-1}×cm^{-1})]: 200 (max, 43642), 224 (shoulder, 10849).

MALDI-TOF-MS calculated for $[C_{42}H_{75}N_3O_3]+H^+$ 670,59 Da, found 670,58 *m/z*.

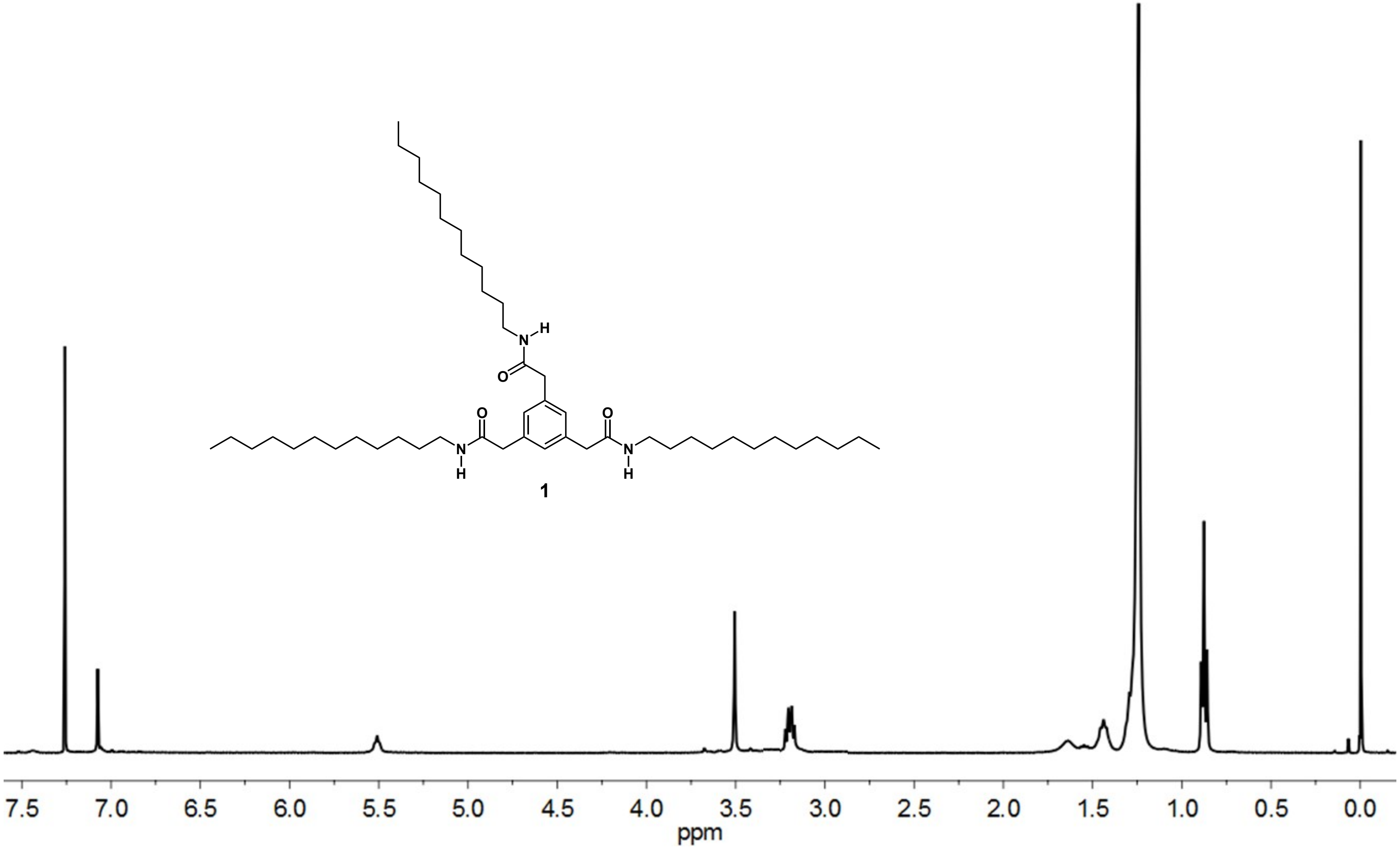

Figure S1. ^{1}H NMR spectrum of **1**.

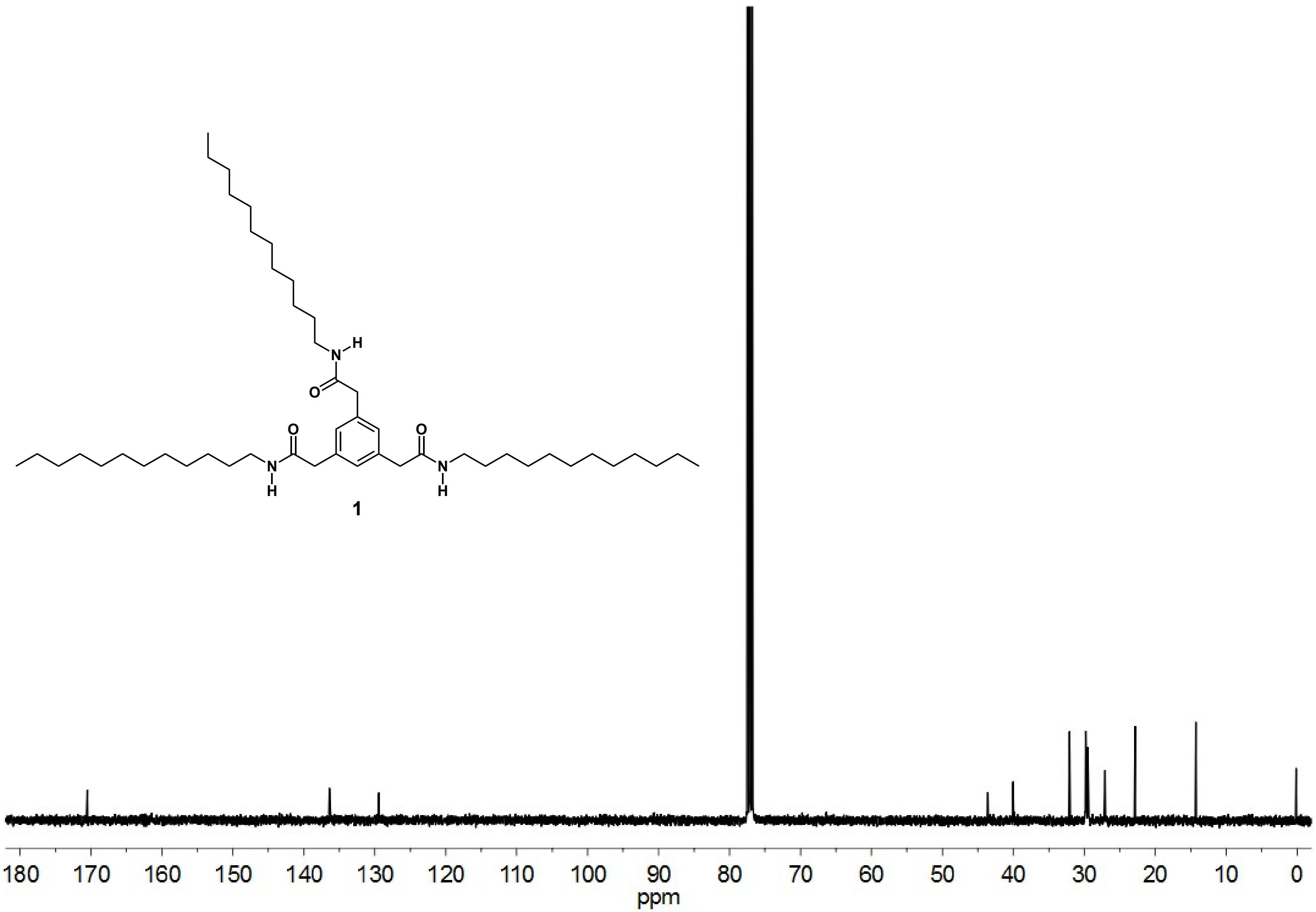

Figure S2. ^{13}C NMR spectrum of **1**.

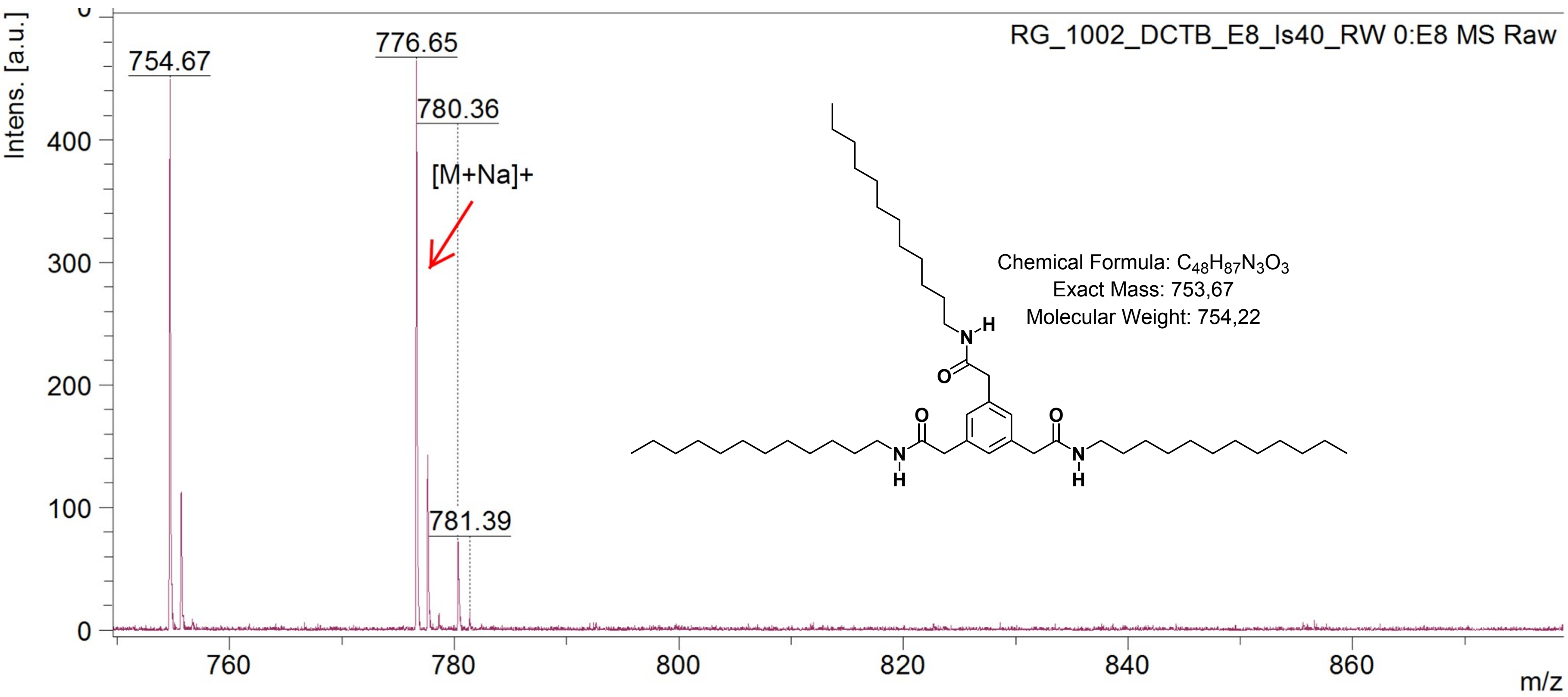

Figure S3. MALDI-TOF mass spectrum (positive mode) of **1**.

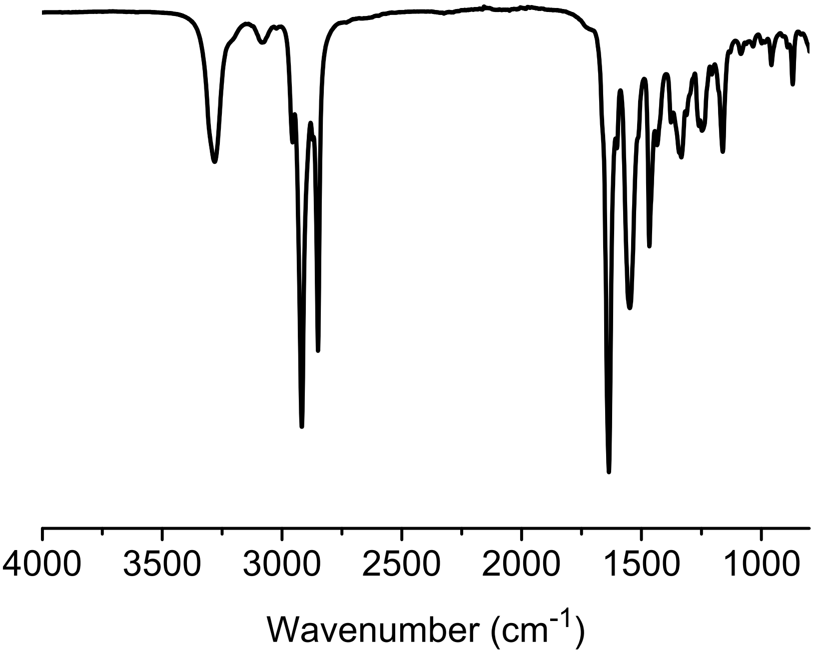

Figure S4. FT-IR spectrum of **1**.

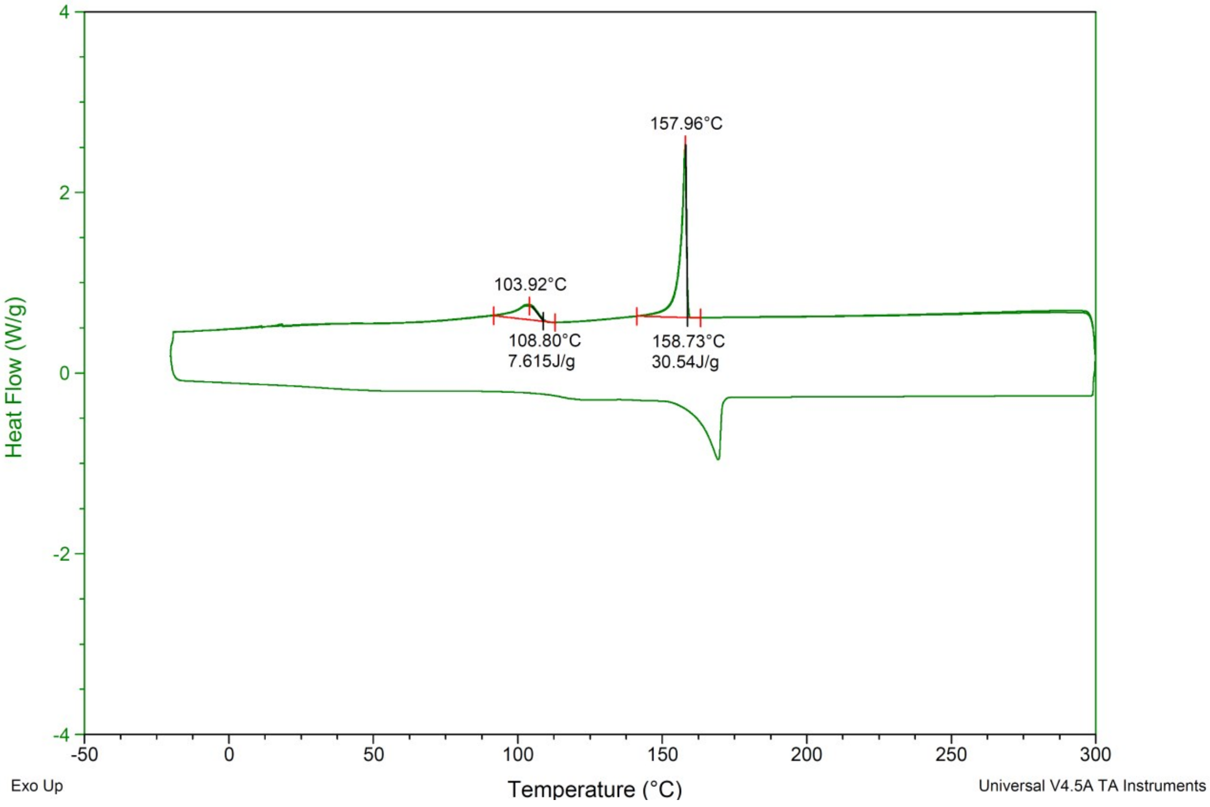

Figure S5. DSC trace (second heating and cooling at 10 ºC/ min) of **1**.

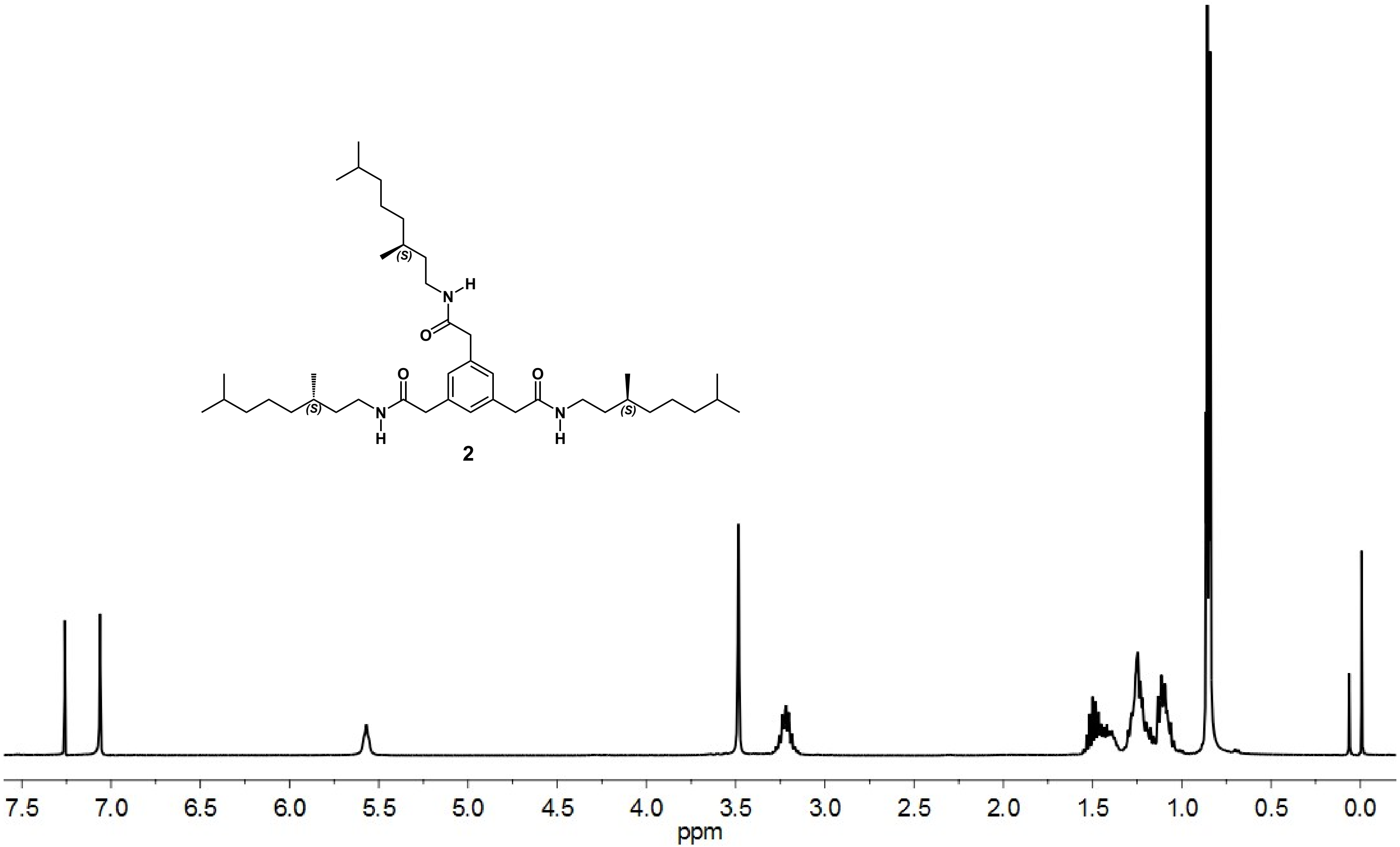

Figure S6. ^{1}H NMR spectrum of **2**.

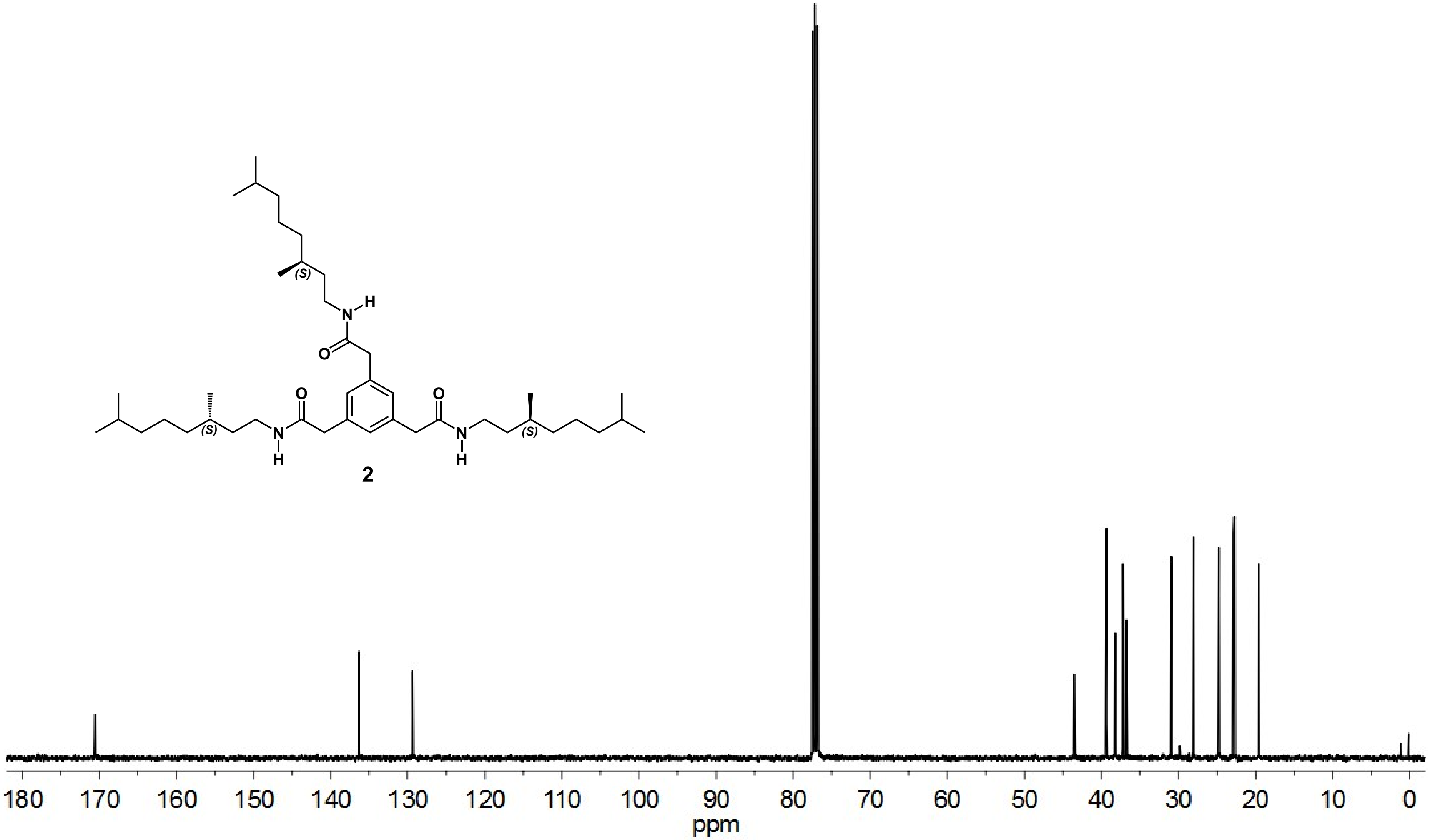

Figure S7. ^{13}C NMR spectrum of **2**.

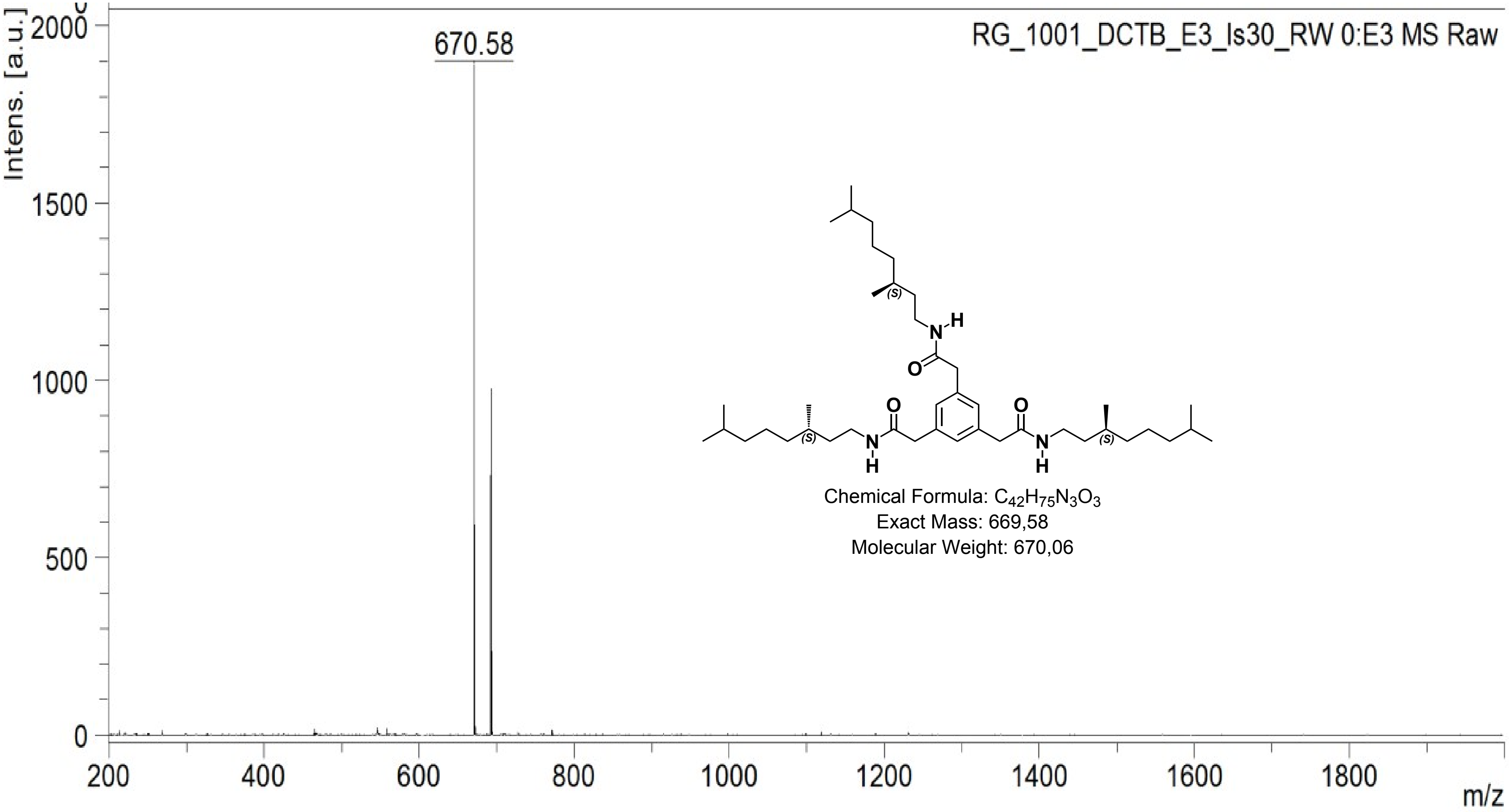

Figure S8. MALDI-TOF mass spectrum (positive mode) of **2**.

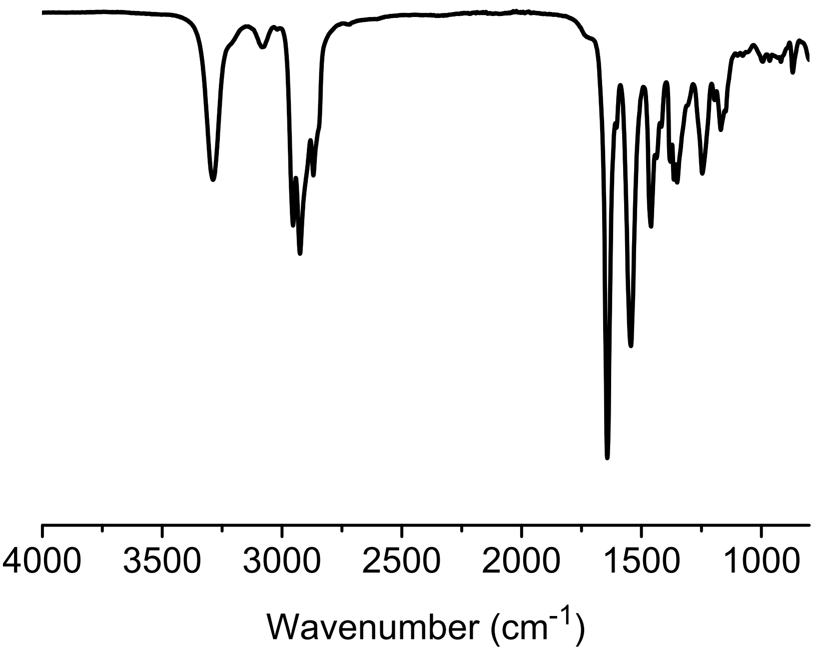

Figure S9. FT-IR spectrum of **2**.

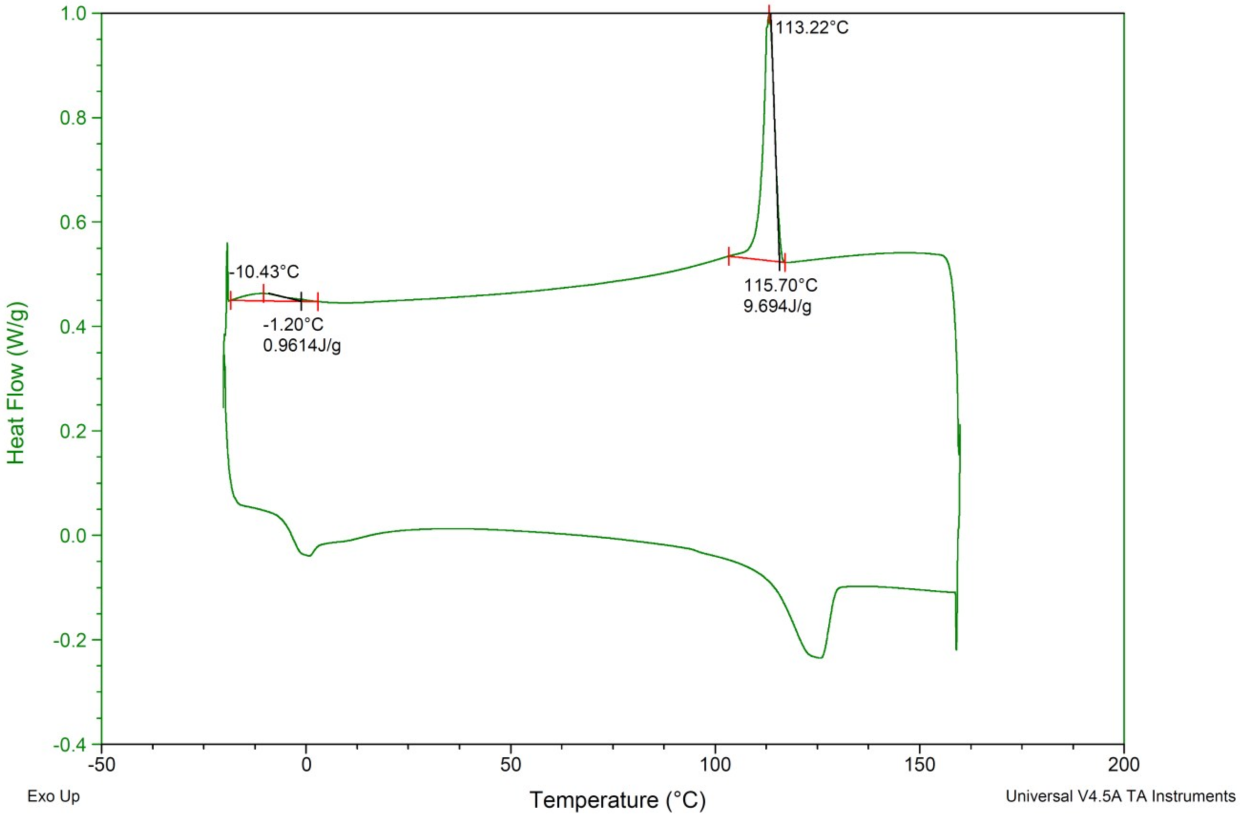

Figure S10. DSC trace (second heating and cooling at 10 ºC/ min) of **2**.

Polarized Optical Microscopy characterization

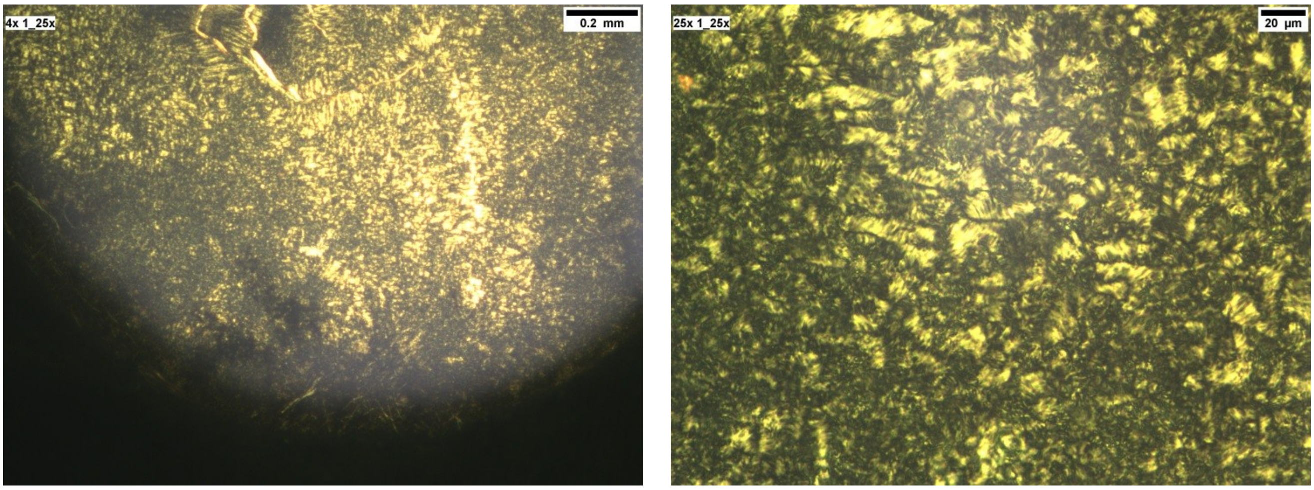

Figure S11. POM micrographs of birefringent textures of **1** obtained at 30 ºC upon slow cooling from the isotropic melt. Scale bars (top right in pictures): 0.2 mm (left) and 20 μm (right).

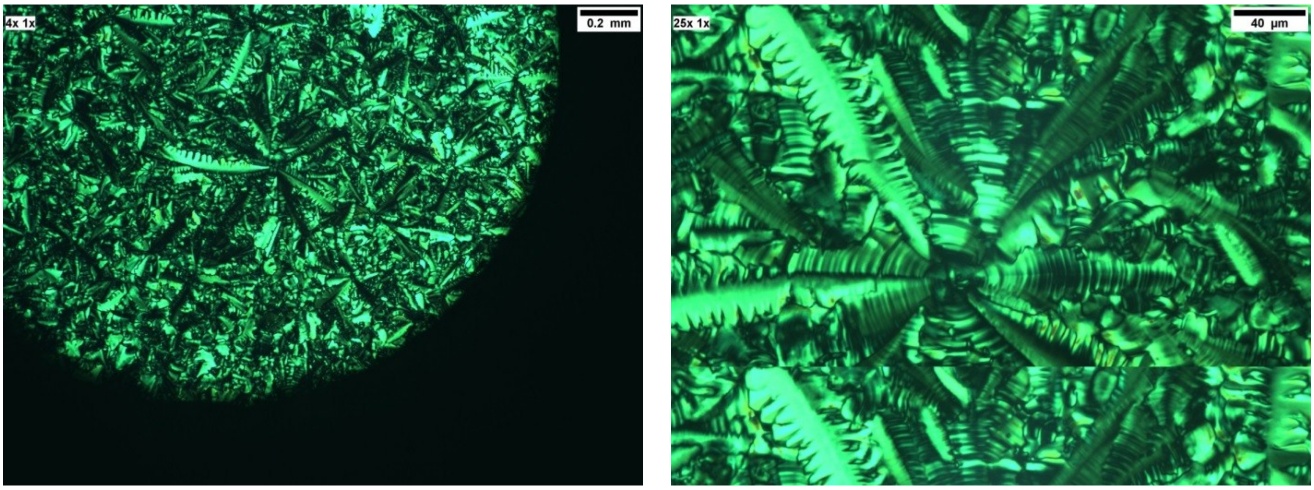

Figure S12. POM micrographs representing the pseudo-focal conic textures of **2** obtained at 30 ºC upon slow cooling (10 °C/min) from the isotropic melt. Scale bars (top right in pictures): 0.2 mm (left) and 40 μm (right).

Temperature Dependent IR

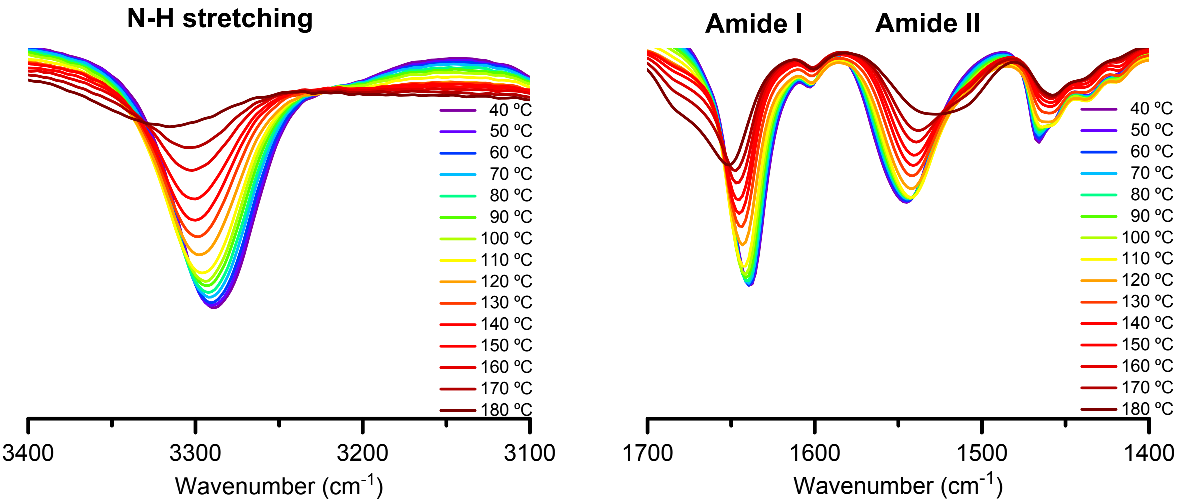

Figure S13. Evolution of the signals of the N-H stretching (left) and Amide I and Amide II vibrations (right) of **1** upon heating.

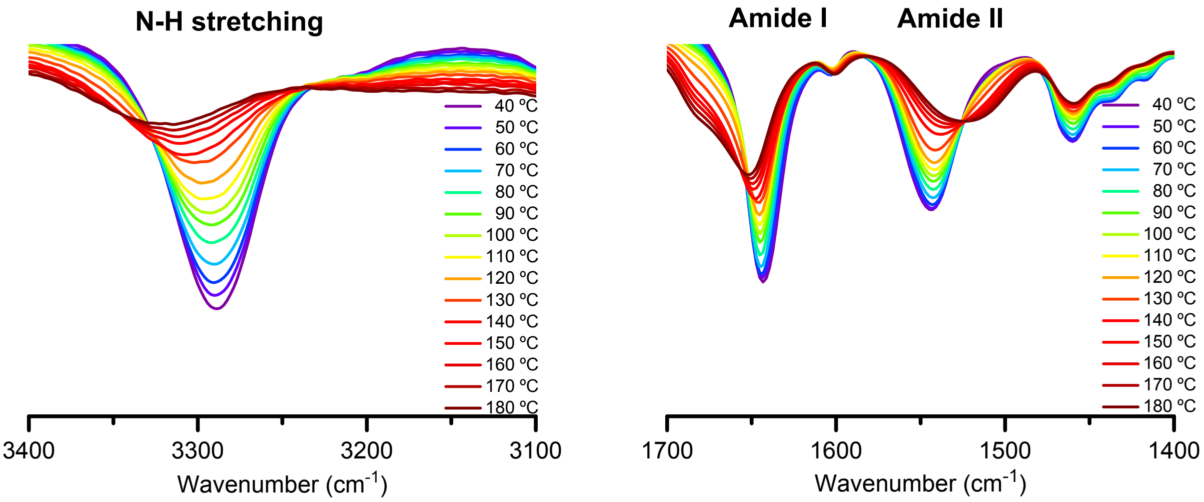

Figure S14. Evolution of the signals of the N-H stretching (left) and Amide I and Amide II vibrations (right) of **2** upon heating.

Concentration dependent gelation studies

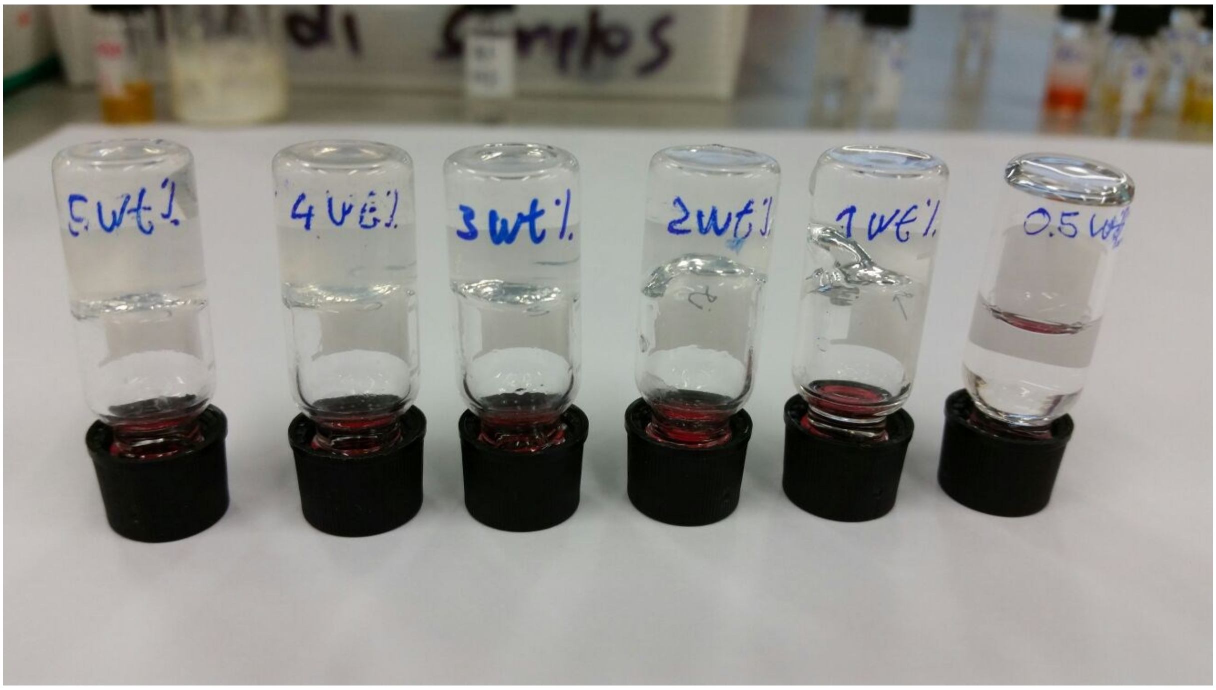

Figure S15. Outcome of gelation experiments in heptane at different concentrations of **2** (from left to right: 5 wt% = 75 mM; 4 wt% = 60 mM; 3 wt% = 45 mM; 2 wt% = 30 mM; 1 wt% = 15 mM; 0.5 wt% = 7.5 mM).

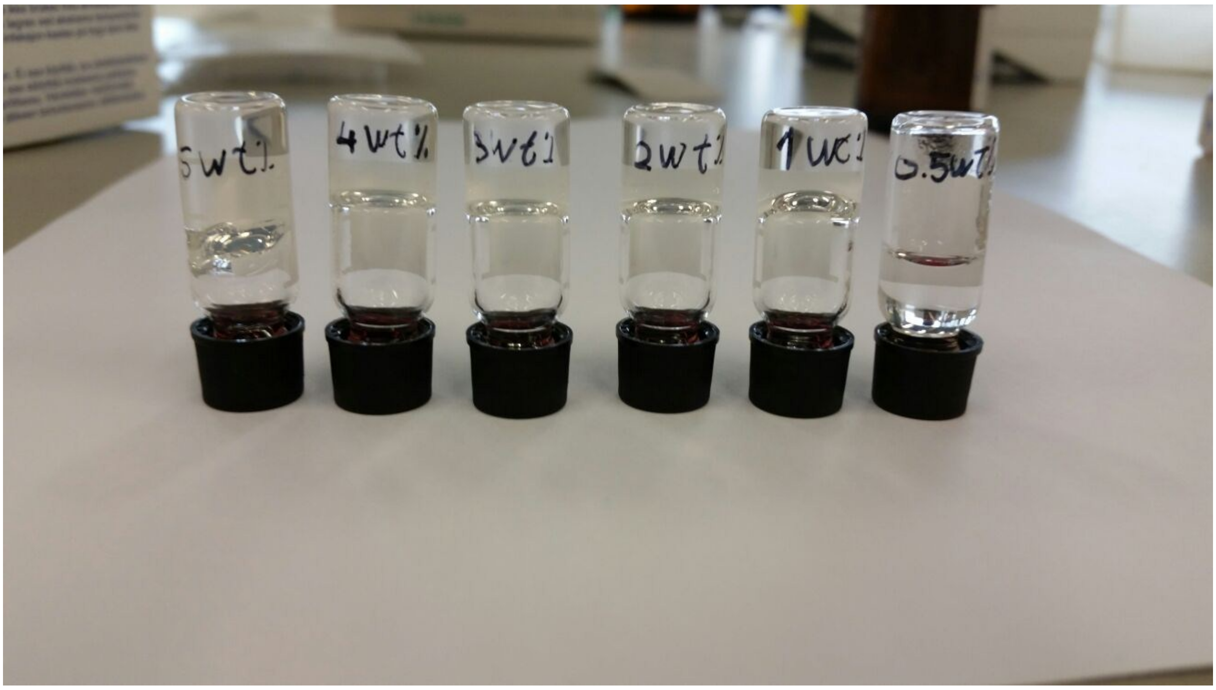

Figure S16. Outcome of gelation experiments in MCH at different concentrations of **2** (from left to right: 5 wt% = 75 mM; 4 wt% = 60 mM; 3 wt% = 45 mM; 2 wt% = 30 mM; 1 wt% = 15 mM; 0.5 wt% = 7.5 mM).

Solution-phase IR

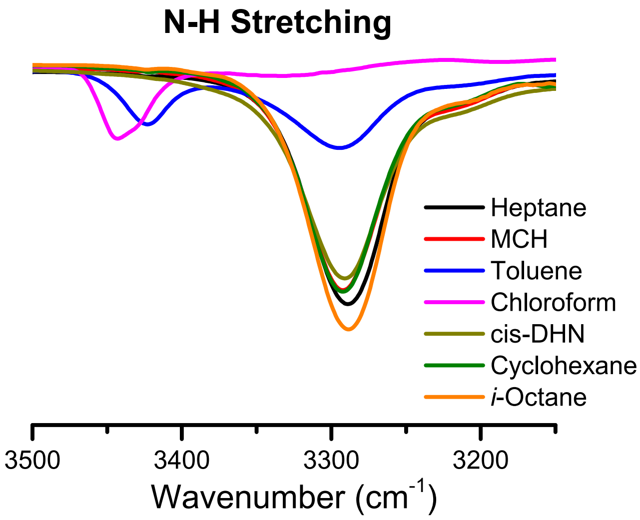

Figure S17. N-H stretching region in solution-phase IR spectra of **2**. In all alkane solvents and partially in toluene, the N-H vibration is shifted to lower wavenumbers/frequencies due to the formation of intermolecular hydrogen bonds, whereas in CHCl$_3$, where mBTAs are molecularly dissolved, the same vibration has a higher energy content.

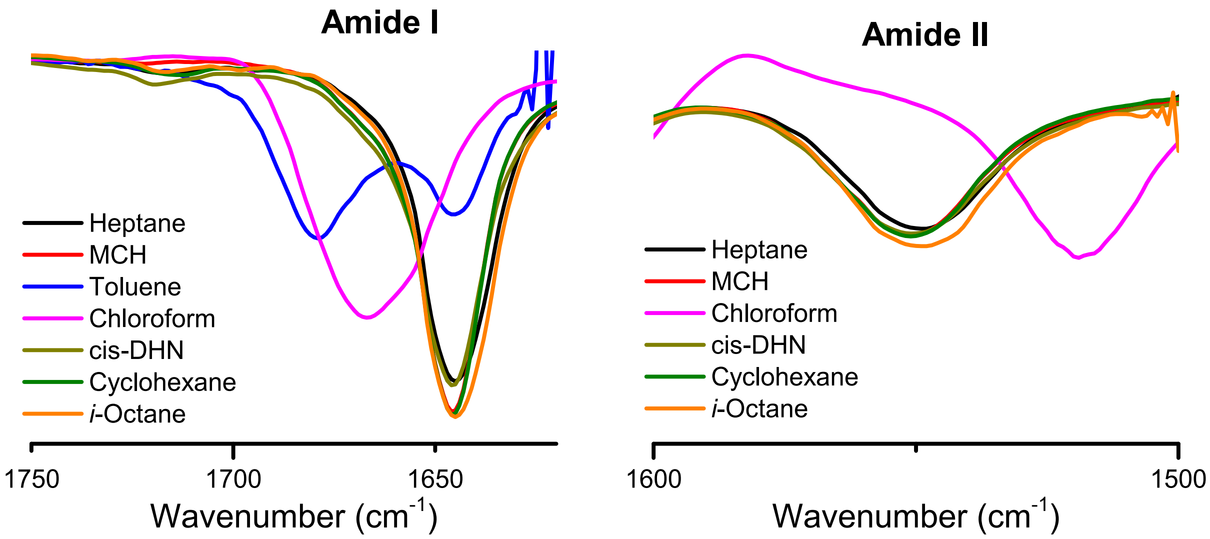

Figure S18. Amide I (left) and amide II (right) regions in solution-phase IR spectra of **2**. The same solvent-dependence trend of Figure S17 is observed for the Amide I vibration, whereas the Amide II has a higher energy content in solvents where mBTAs are self-assembled. In the Amide II region the spectrum in toluene is omitted for clarity, as it was extremely noisy in such solvent.

Study of the self-assembly of 2 in MCH with ^{1}H NMR spectroscopy

Qualitative proof of the self-assembly of **2** in MCH at 5 mM was obtained with proton Nuclear Magnetic Resonance spectroscopy (^{1}H-NMR). Progressive broadening and disappearance of the signals of the aromatic protons (red circle), the N-H (blue circle), the benzylic-type -CH_2 (green circle) and the -CH_2 adjacent to the amide nitrogen atom (grey circle) occurred at temperatures ≤ 40 °C upon cooling from 90 °C, suggesting longer correlation times caused by larger molar volumes and increased solution viscosity.[1]

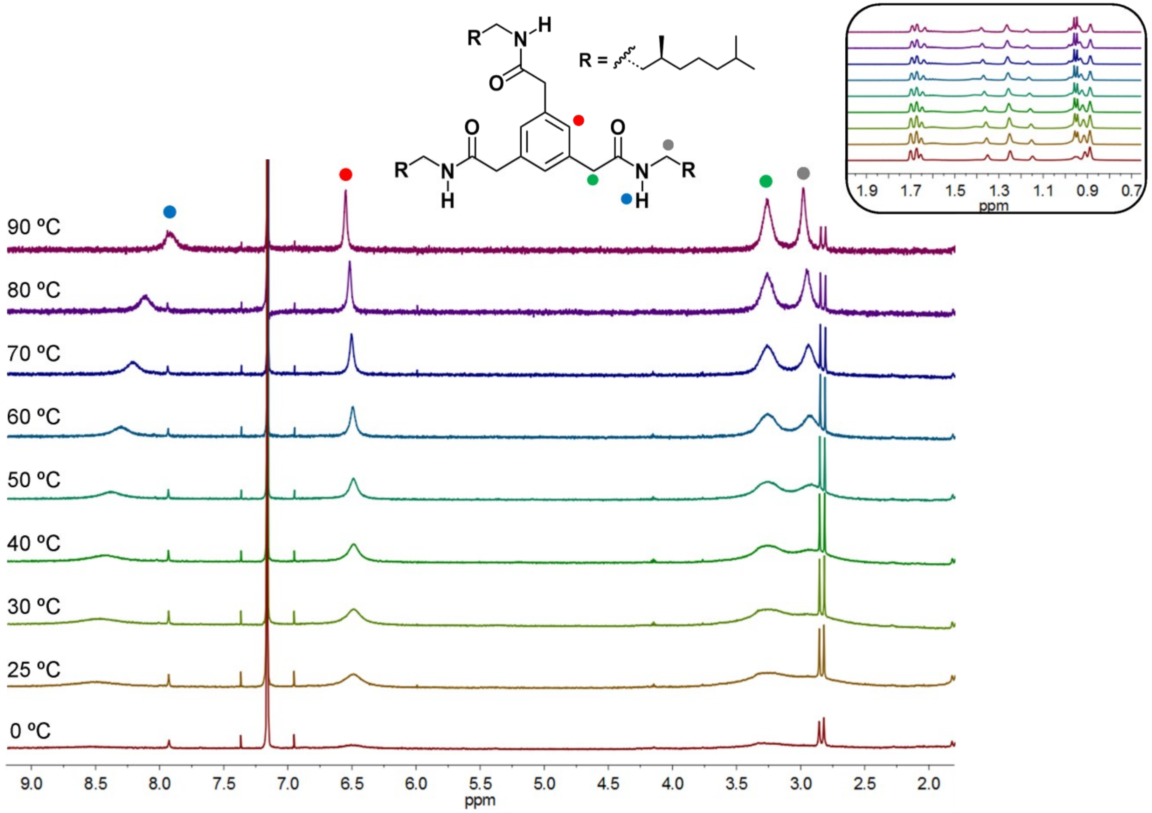

Figure S19. Temperature depent self assembly of **2** (5 mM) in deuterated MCH followed by ^{1}H NMR spectroscopy (500 MHz). The signals of the aromatic protons, the N-$\underline{H}$, the benzylic-type -$C\underline{H}_2$ and the-$C\underline{H}_2$ adjacent to the amide nitrogen atom are labeled. The alkyl region is shown in the inset.

Transmission Electron Microscopy characterization

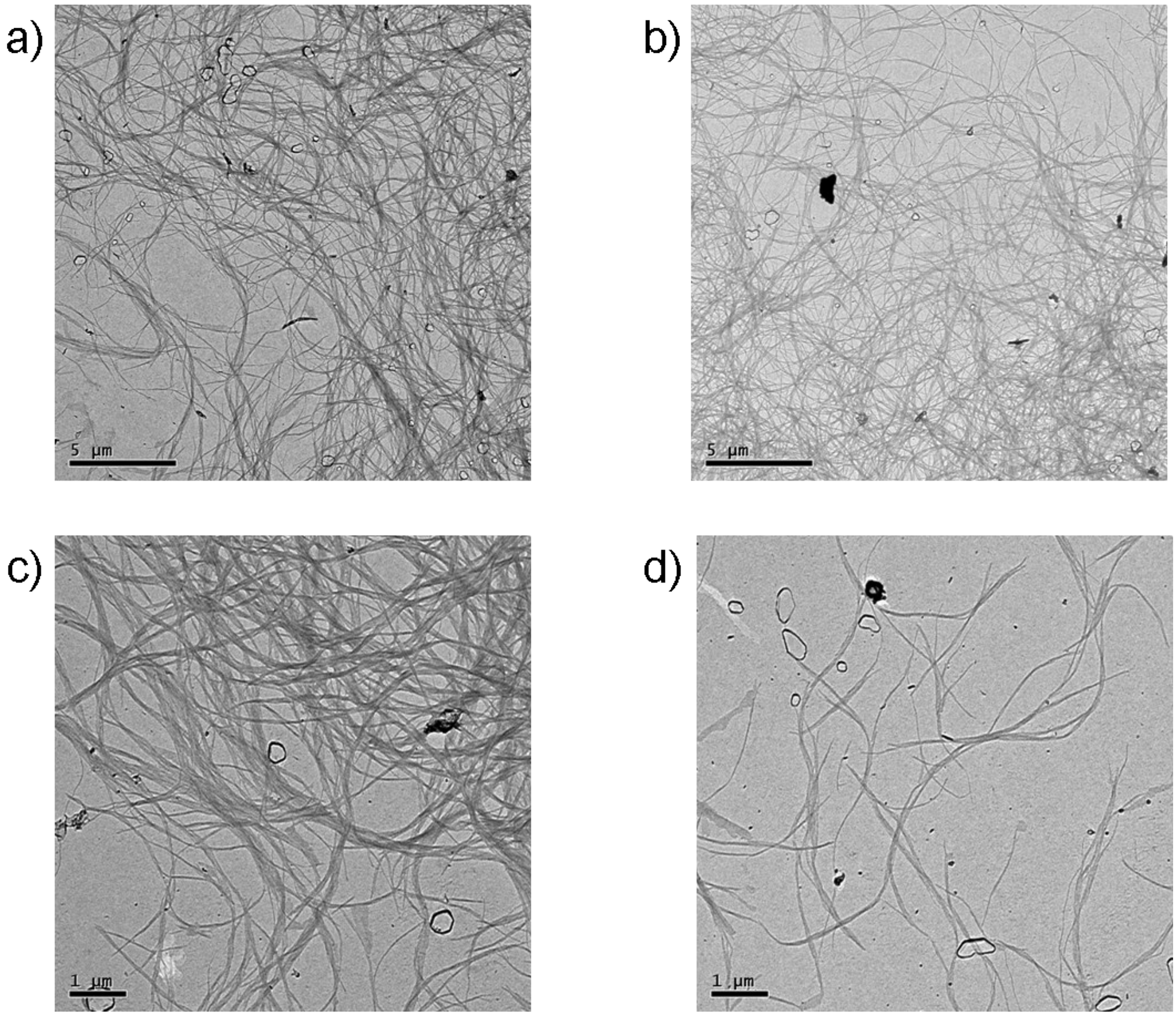

Figure S20. TEM micrographs showing long and thin supramolecular fibers obtained from 7.5 mM solutions of **2** in heptane at different magnifications. Scale bars (bottom left) are 5 μm for a) and b), 1 μm for c) and d).

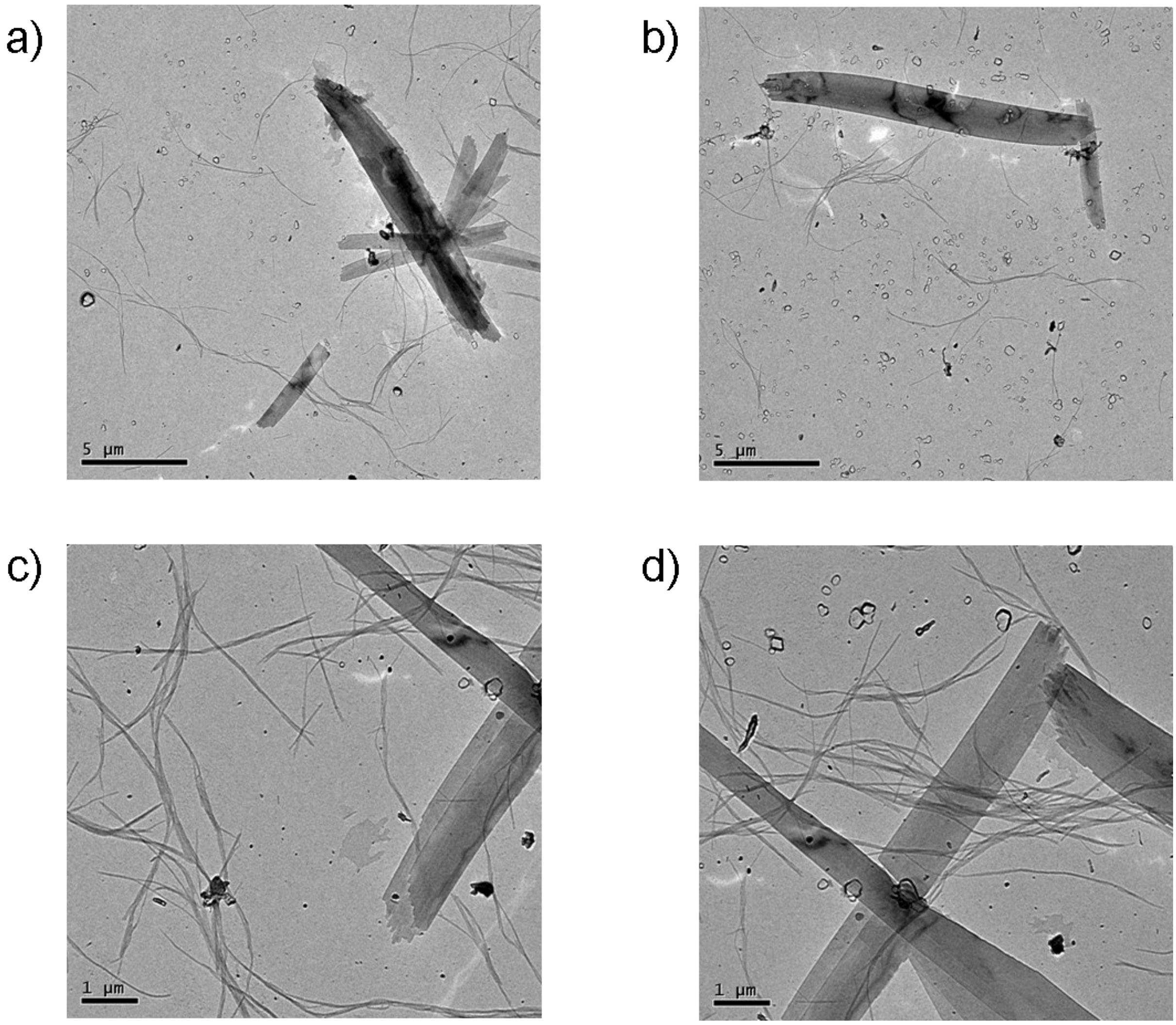

Figure S21. TEM micrographs showing the coexistence of thin supramolecular fibers and ribbon-like architectures in 7.5 mM solutions of **2** in MCH at different magnifications. Scale bars (bottom left) are 5 μm for a) and b), 1 μm for c) and d).

UV-vis and CD spectra

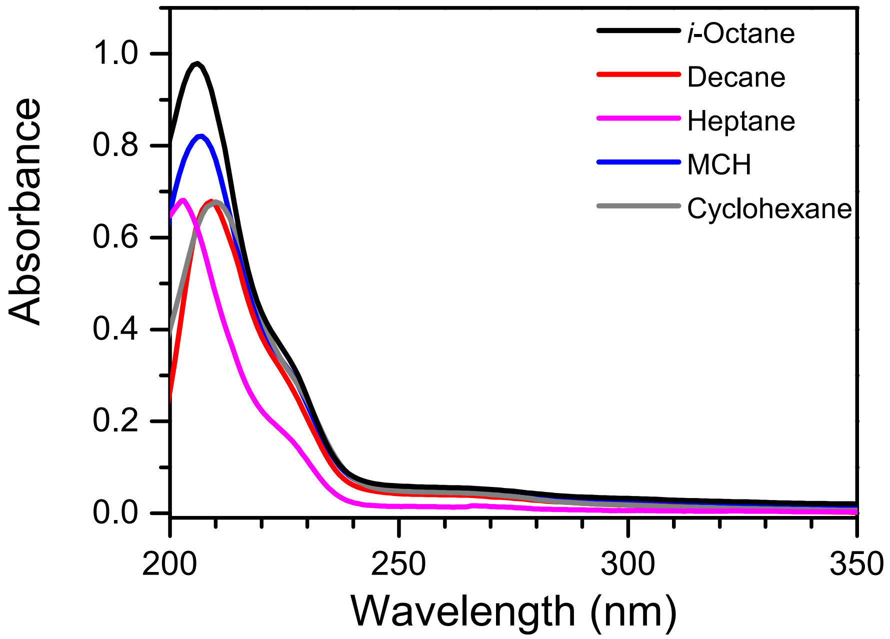

Figure S22. UV-Vis spectra of **2** at 30 μM concentration (optical path = 1 cm).

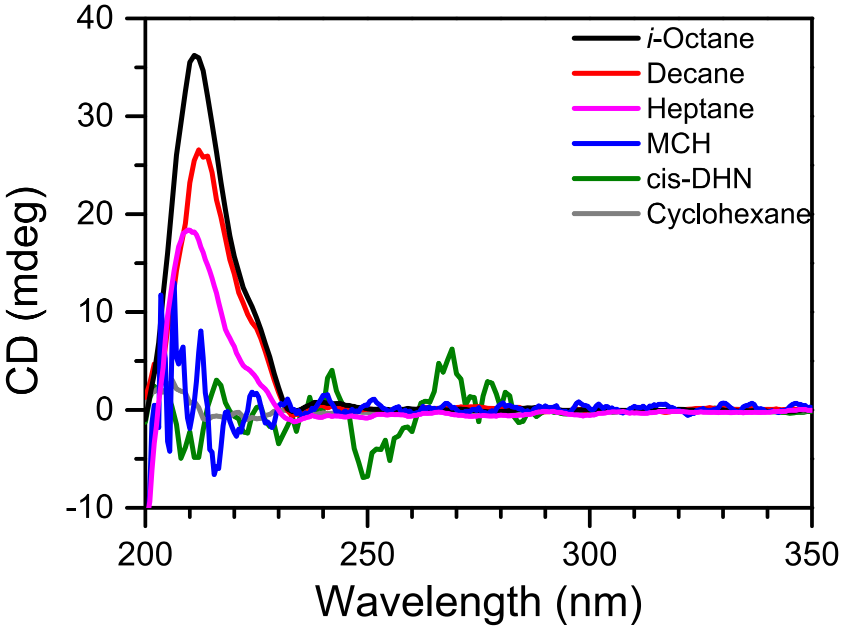

Figure S23. CD spectra of **2** at 30 μM concentration (optical path = 1 cm). CD-silent spectra are measured in cyclic solvents (MCH, cyclohexane and cis-decaline).

Temperature Dependent UV-vis and CD spectra in Heptane

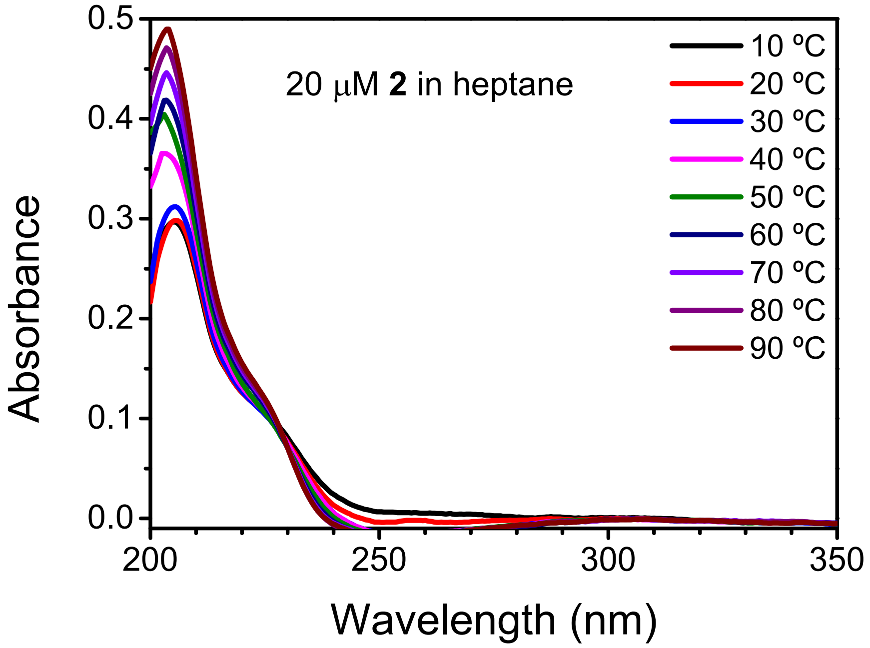

Figure S24. TD-UV-Vis spectra of **2** at 20 μM concentration in Heptane (optical path = 1 cm).

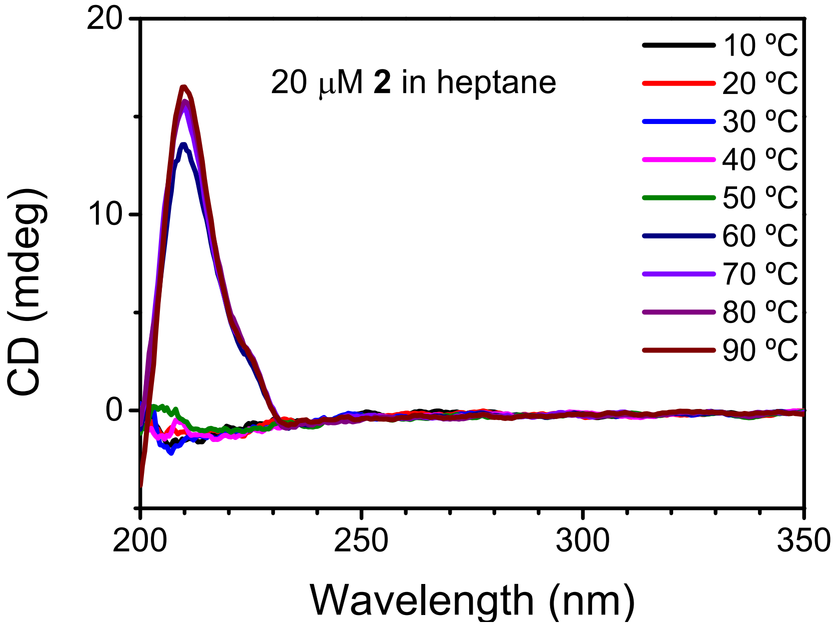

Figure S25. TD-CD spectra of **2** at 20 μM concentration in Heptane (optical path = 1 cm).

Dynamic Light Scattering characterization

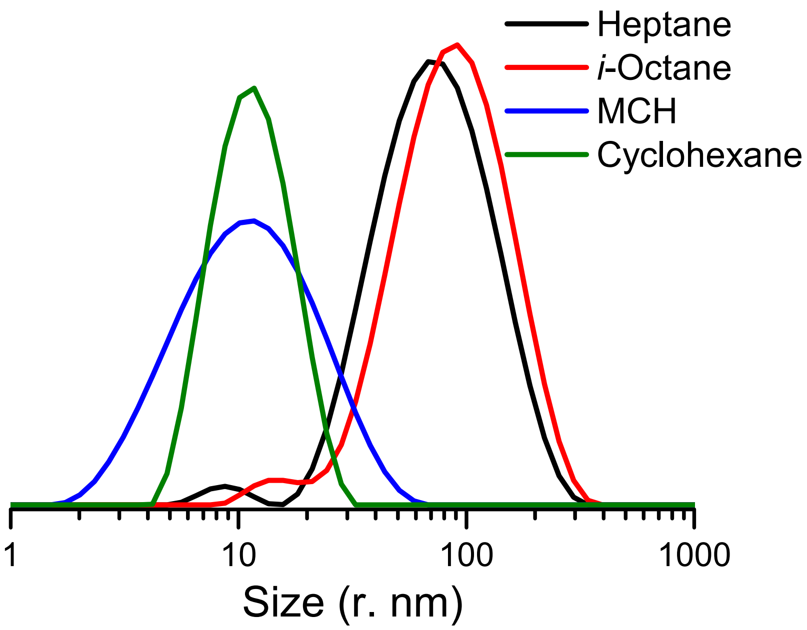

Figure S26. Size distribution of aggregates formed in the supramolecular polymerization of **2** (5×10^{-5}M, 20 °C) in a number of alkane solvents. Larger aggregates are always obtained with linear and branched aliphatic solvents. The aggregates were detected with DLS at a 90 ° detection angle.

Computational section

Computational details

Molecular mechanics and Molecular dynamics simulation. Ground state geometry of **2** was optimized at the B3LYP-D3/6-31+G(d,p) level of theory. Quantum optimized geometries were used to calculate RESP atomic charges by fitting the electrostatic potential obtained from the formalism from Duan et al.[2]

Fitting process was carried out using R.E.D.[3] and Gaussian09[4] softwares. Force field parameters were derived from Generalized Amber Force Field (GAFF)[5] using Antechamber program.[6]

Methylcyclohexane (MCH) and heptane (HEP) solvent parameters were both derived from B3LYP/6-311+G(d,p) quantum calculations. Partial atomic charges were also derived from RESP atomic charges using Duan et al. formalism. 10 ns Molecular dynamic simulations were performed on boxes containing only MCH or HEP in order to ensure the validity of MCH and HEP parameters.

P- and M-Helices were built for both 3:0 and 2:1 H-bonding networks using the Avogadro package.[7] Such models were then minimized using the Amber14 package.[8] Then, helices were solvated in rectangular boxes by adding either 2418 HEP molecules or 2778 MCH molecules. Such boxes were first thermalized by performing 50ps MD simulations. Then, 100ps NPT MD simulations were performed to equilibrate box size according to densities of ca. 0.68 g.cm^{-3} and 0.76 g.cm^{-3}, respectively in HEP and MCH. After equilibration, box size were ca. 74x74x117 Å for both types of solvent. Finally, Æ40ns NPT MD production simulations were carried out at 300K. Conformational analyses were performed using the cpptraj software.[9] ECD calculations were performed on 100 snapshots extracted from the last 10ns MD simulations.

Semi-empirical CD calculations. The calculation of excitonic CD spectra proceeds in two steps. First the lowest 60 excited states of the molecules involved in the helices are computed at the INDO/SCI level[10] using an active space of 25 occupied and 25 virtual molecular orbitals. Then, an excitonic Hamiltonian encompassing a 25xN basis functions (with N the aggregate size) is built on the basis of INDO/SCI excitation energies and exciton couplings. The latter are calculated as Coulomb interactions between transition denisities, thus going beyong the usual dipole model.[11]

Quantum mechanics calculations in vacuum. Ground state Potential energy surface of 2-phenylacetamide was performed at the B3LYP-D3/SV(P) using Becke-Johnson damping function.[12] DFT calculations were carried out using the Gaussian09 package

MD Results

Table S1. Average *m*BTA-*m*BTA interaction energies per *m*BTA ($E_{m\mathrm{BTA}\text{-}m\mathrm{BTA}}$, kcal.mol^{-1}.molecule^{-1}), average solvent-stack interaction energies per *m*BTA ($E_{m\mathrm{BTA\text{-}solvent}}$, kcal.mol^{-1}.molecule^{-1}) and average total interaction energies per *m*BTA for P- and M-helices in (a) heptane and (b) methylcyclohexane.

(a)

	P-Helix		M-Helix	
	3:0	*2:1*	*3:0*	*2:1*
$E_{m\mathrm{BTA}\text{-}m\mathrm{BTA}}$	-31.1	-30.6	-31.7	-30.7
$E_{m\mathrm{BTA\text{-}solvent}}$	-41.1	-42.7	-39.2	-41.7
E_{int}	-71.0	-72.0	-69.6	-71.1

(b)

	P-Helix		M-Helix	
	3:0	*2:1*	*3:0*	*2:1*
$E_{m\mathrm{BTA}\text{-}m\mathrm{BTA}}$	-28.8	-28.7	-29.7	-28.9
$E_{m\mathrm{BTA\text{-}solvent}}$	-43.4	-46.4	-44.2	-46.7
E_{int}	-71.0	-74.0	-72.7	-74.5

Figure S27. H-bond distance distributions for P- and M-helices in (a) heptane and (b) methylcyclohexane.

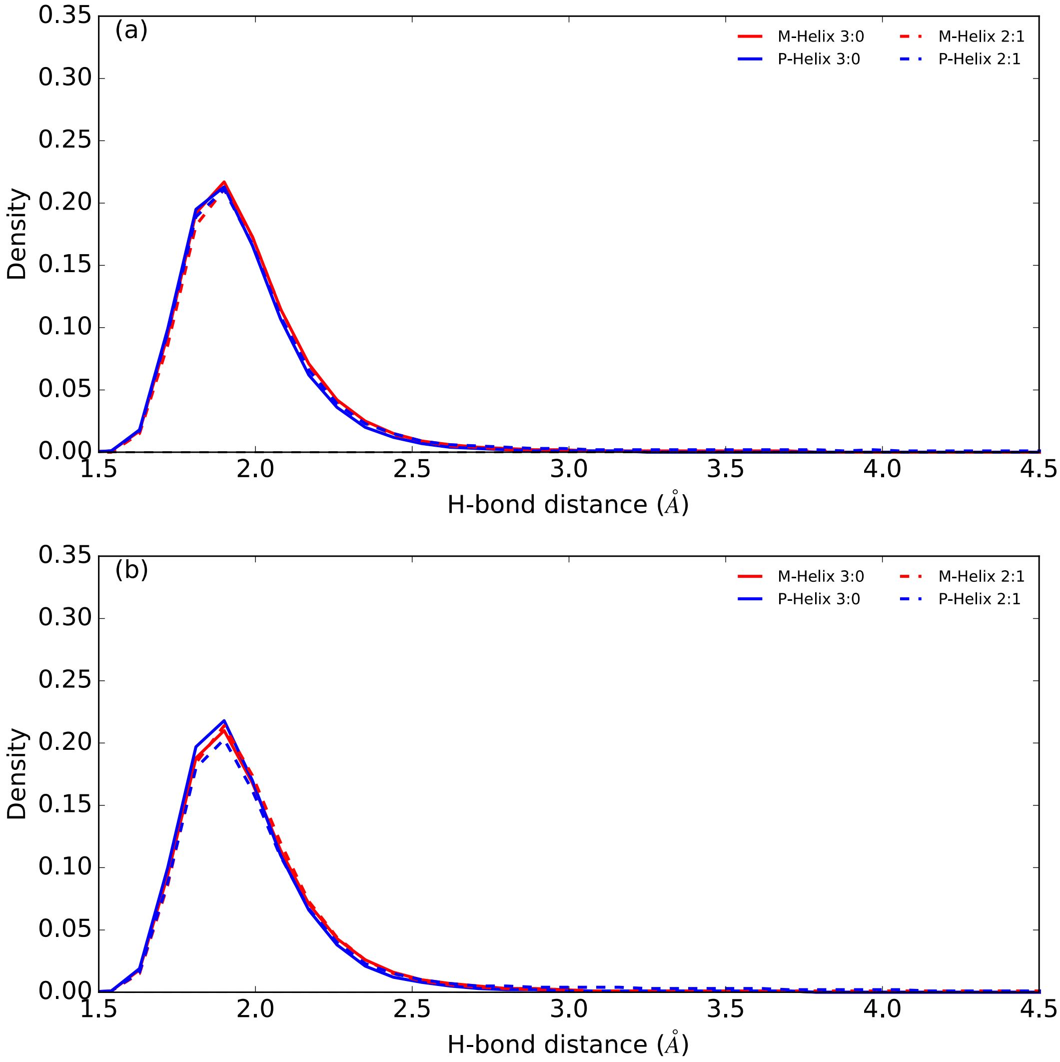

Figure S28. Rise distributions for P- and M-helices in (a) heptane and (b) methylcyclohexane.

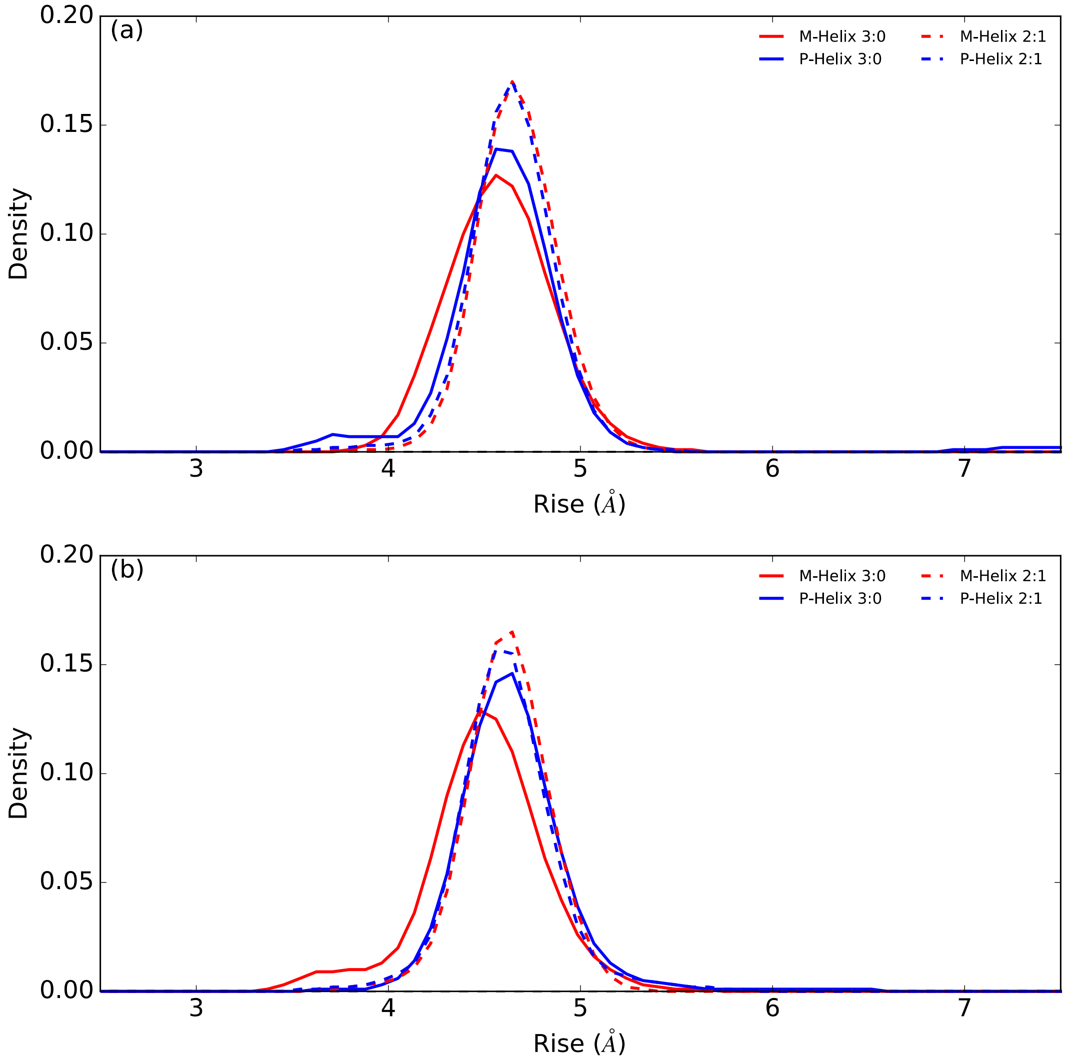

Figure S29. Twist distributions for P- and M-helices in (a) heptane and (b) methylcyclohexane.

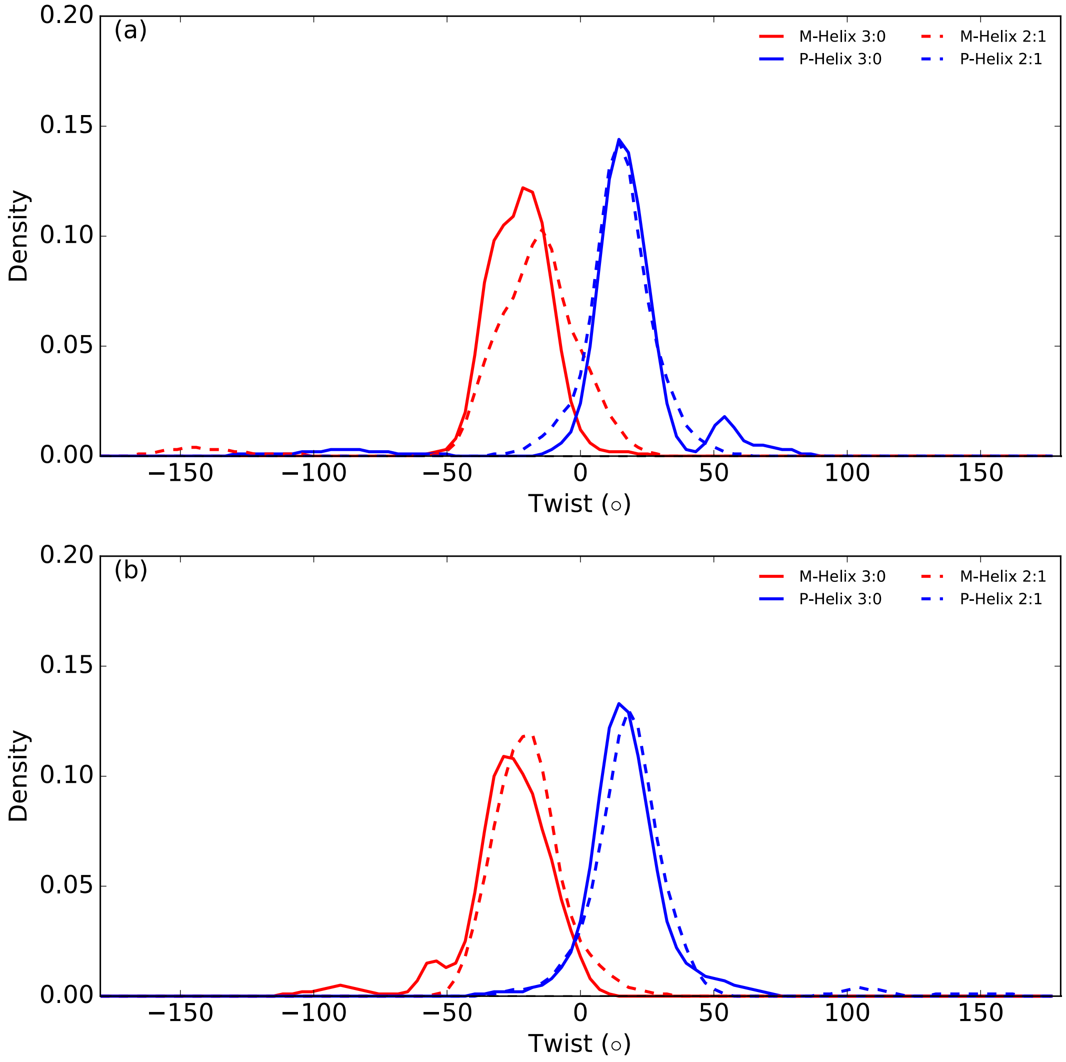

Figure S30. ϕ dihedral angle distributions for P- and M-helices in (a) heptane and (b) methylcyclohexane

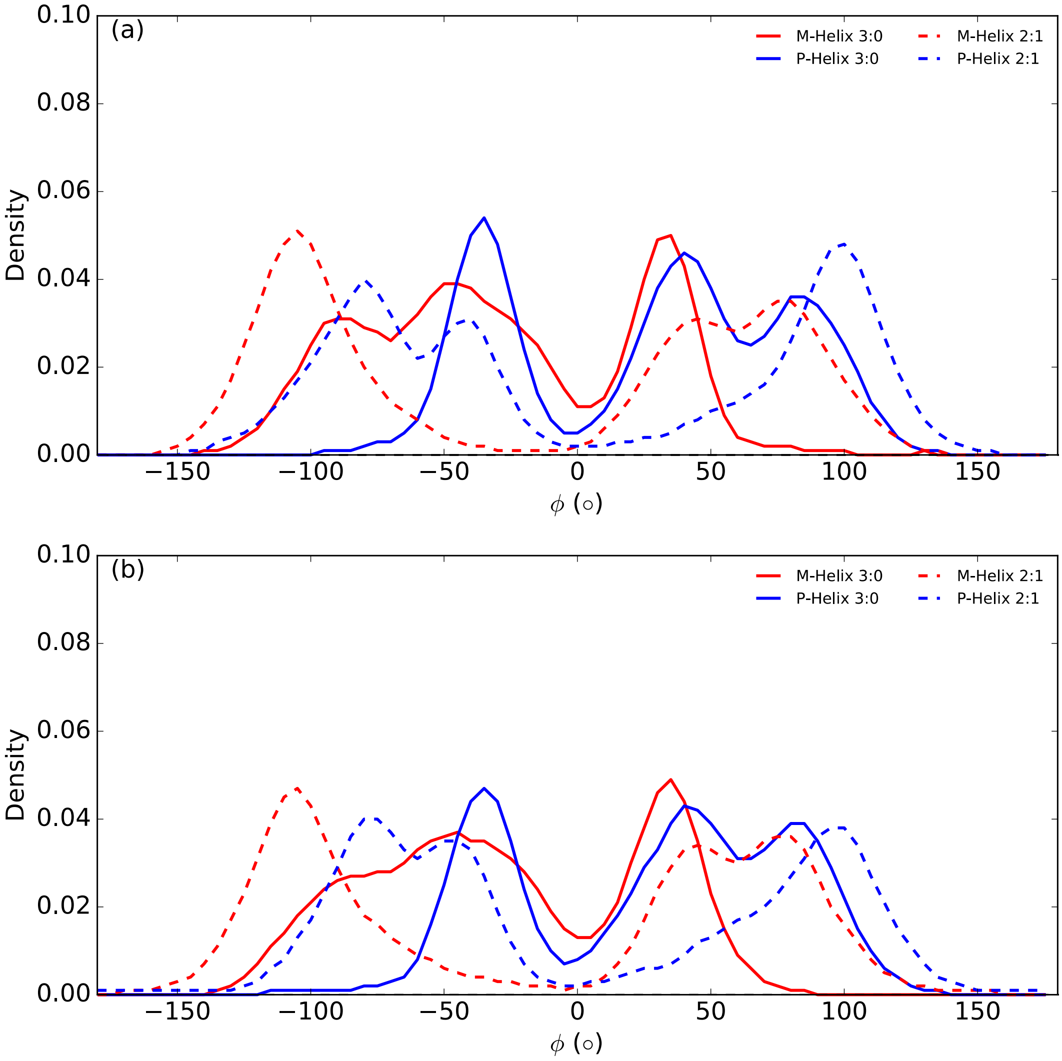

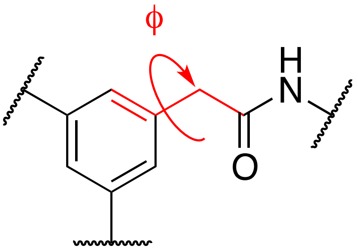

Figure S31. ψ dihedral angle distributions for P- and M-helices in (a) heptane and (b) methylcyclohexane

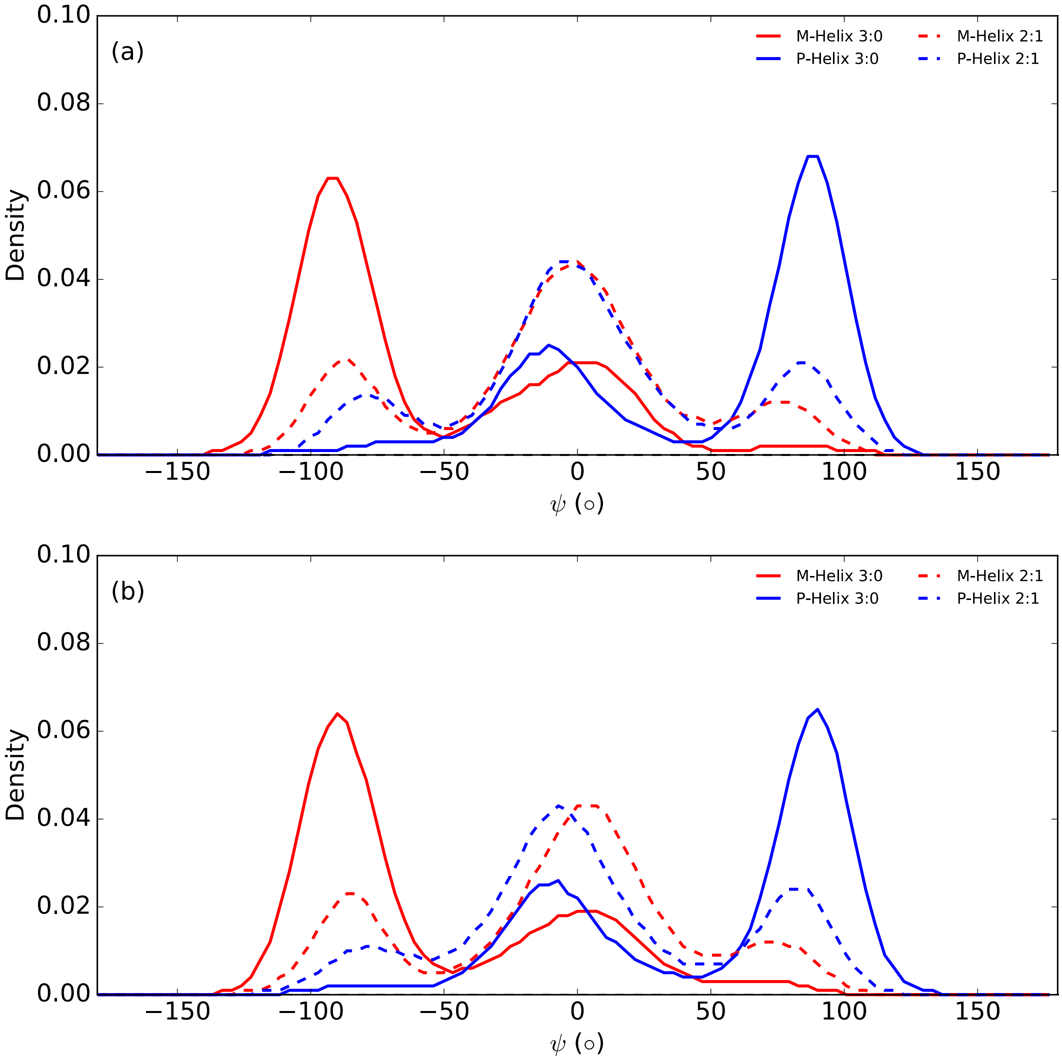

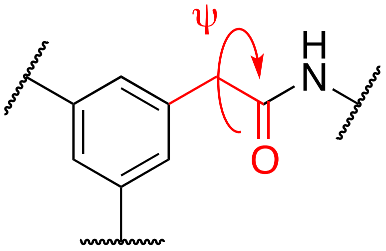

Figure S32. Theoretical UV/Vis absorption spectra of P- and M-helix of **2** in heptane adopting (a) 3:0 and (b) 2:1 configuration as well as in MCH adopting (c) 3:0 and (d) 2:1 configurations.

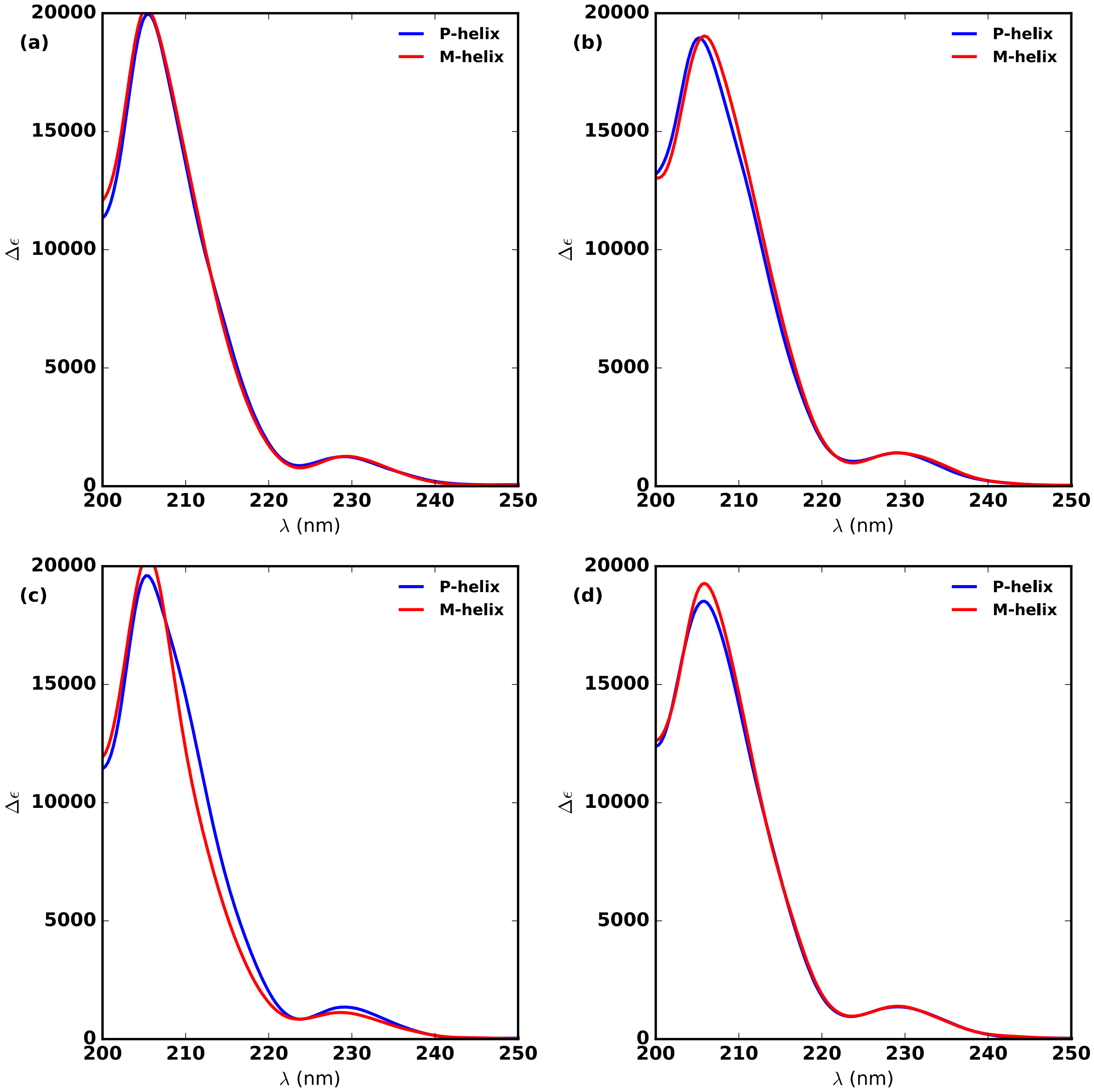

Figure S33 Representative snapshot of 25-mer stack (left) and zoom on central units (right) of 2:1 conformation assembling in a M-helix fashion (side chain hydrogen atoms are omitted for sake of clarity).

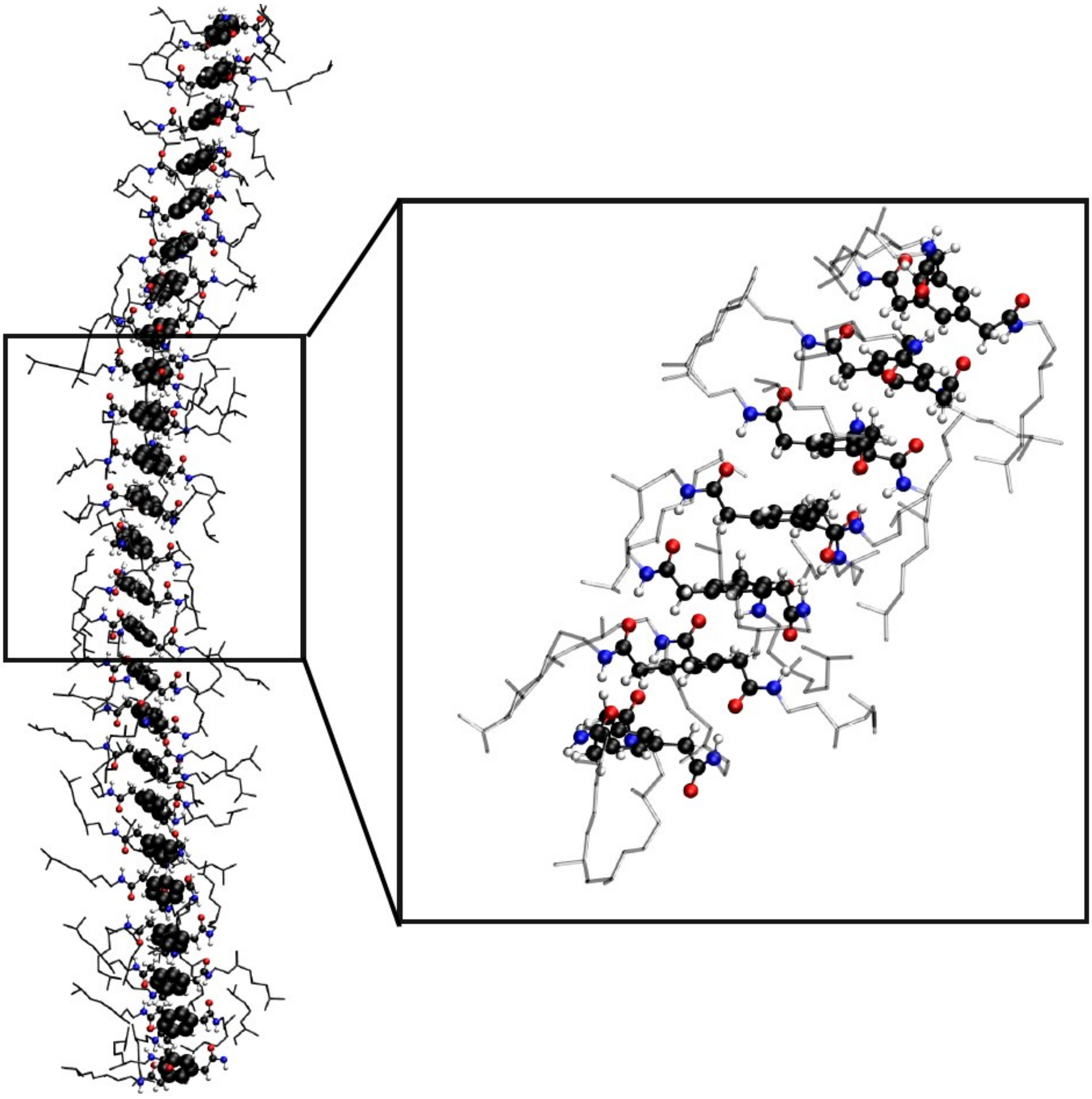

QM Results

Figure S34. Potential energy surface of phi and psi dihedral angle on N-methyl-2-phenylacetamide performed at the B3LYP/6-31+G(d,p) level of theory. Except for the three high points on the potential energy surface corresponding to sterically hindered conformations, the rest of the PES is quite flat with barriers lower than 3-4 kcal/mol.

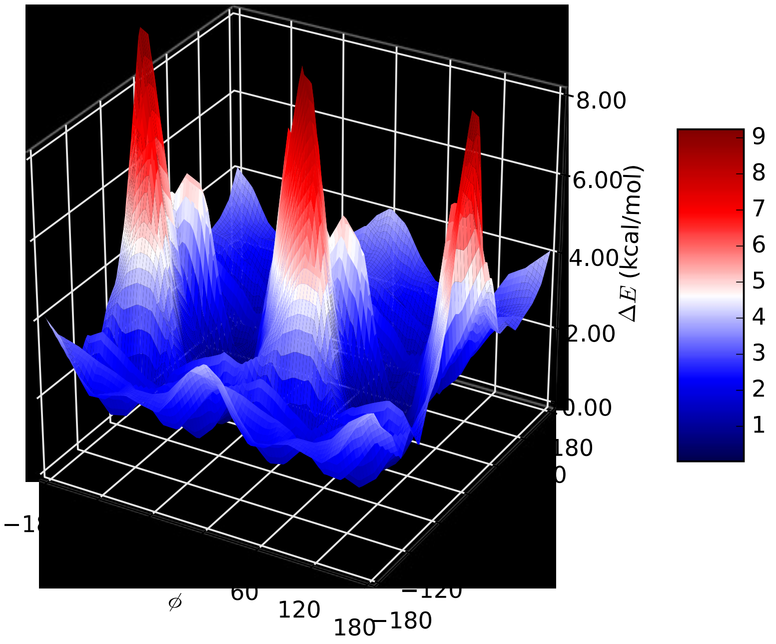

References

---

[1] NMR of polymers, Academic Press, F. A. Bovey and P. A. Mirau.

[2] Y. Duan, C. Wu, S. Chowdhury, M. C. Lee, G. Xiong, W. Zhang, R. Yang, P. Cieplak, R. Luo, T. Lee, J. Caldwell, J. Wang and P. Kollman, *J. Comput. Chem.*, 2003, **24**, 1999–2012.

[3] F.-Y. Dupradeau, A. Pigache, T. Zaffran, C. Savineau, R. Lelong, N. Grivel, D. Lelong, W. Rosanski and P. Cieplak, *Phys. Chem. Chem. Phys. PCCP*, 2010, **12**, 7821–7839.

[4] M. J. Frisch, G. W. Trucks, H. B. Schlegel, G. E. Scuseria, M. A. Robb, J. R. Cheeseman, G. Scalmani, V. Barone, B. Mennucci, G. A. Petersson, H. Nakatsuji, M. Caricato, X. Li, H. P. Hratchian, A. F. Izmaylov, J. Bloino, G. Zheng, J. L. Sonnenberg, M. Hada, M. Ehara, K. Toyota, R. Fukuda, J. Hasegawa, M. Ishida, T. Nakajima, Y. Honda, O. Kitao, H. Nakai, T. Vreven, J. A. Montgomery Jr., J. E. Peralta, F. Ogliaro, M. J. Bearpark, J. Heyd, E. N. Brothers, K. N. Kudin, V. N. Staroverov, R. Kobayashi, J. Normand, K. Raghavachari, A. P. Rendell, J. C. Burant, S. S. Iyengar, J. Tomasi, M. Cossi, N. Rega, N. J. Millam, M. Klene, J. E. Knox, J. B. Cross, V. Bakken, C. Adamo, J. Jaramillo, R. Gomperts, R. E. Stratmann, O. Yazyev, A. J. Austin, R. Cammi, C. Pomelli, J. W. Ochterski, R. L. Martin, K. Morokuma, V. G. Zakrzewski, G. A. Voth, P. Salvador, J. J. Dannenberg, S. Dapprich, A. D. Daniels, Ö. Farkas, J. B. Foresman, J. V. Ortiz, J. Cioslowski and D. J. Fox, *Gaussian 09*, Gaussian, Inc., Wallingford, CT, USA, 2009.

[5] J. Wang, R. M. Wolf, J. W. Caldwell, P. A. Kollman and D. A. Case, *J. Comput. Chem.*, 2004, **25**, 1157–1174.

[6] J. Wang, W. Wang, P. A. Kollman and D. A. Case, *J. Mol. Graph. Model.*, 2006, **25**, 247–260.

[7] M. D. Hanwell, D. E. Curtis, D. C. Lonie, T. Vandermeersch, E. Zurek and G. R. Hutchison, *J. Cheminformatics*, 2012, **4**, 1–17.

[8] D. A. Case, V. Babin, J. Berryman, R. M. Betz, Q. Cai, D. S. Cerutti, C. Iii, T. E, T. A. Darden, R. E. Duke, H. Gohlke, A. W. Goetz, S. Gusarov, N. Homeyer, P. Janowski, J. Kaus, I. Kolossváry, A. Kovalenko, T. S. Lee, S. LeGrand, T. Luchko, R. Luo, B. Madej, K. M. Merz, F. Paesani, D. R. Roe, A. Roitberg, C. Sagui, R. Salomon-Ferrer, G. Seabra, C. L. Simmerling, W. Smith, J. Swails, R. C. Walker, J. Wang, R. M. Wolf, X. Wu and P. A. Kollman, *Amber 14*, University of California, San Francisco, 2015.

[9] D. R. Roe and T. E. Cheatham, *J. Chem. Theory Comput.*, 2013, **9**, 3084–3095.

[10] J. Ridley and M. Zerner, *Theor. Chim. Acta*, 1973, **32**, 111–134.

[11] D. Beljonne, J. Cornil, R. Silbey, P. Millié and J. L. Brédas, *J. Chem. Phys.*, 2000, **112**, 4749–4758.

[12] S. Grimme, S. Ehrlichand L. Goerigk, Effect of the damping function in dispersion corrected density functional theory. *J. Comput. Chem.* 2011, **32**, 1456-1465.